J. Fluid Mech. (2007), *vol.* 578, *pp.* 1–34.
doi:10.1017/S0022112007004922 Printed in the United Kingdom

Strong and weak blow-up of the viscous dissipation rates for concentrated suspensions

LEONID BERLYAND[1] AND ALEXANDER PANCHENKO[2]

[1]Department of Mathematics and Materials Research Institute, Penn State University, University Park, PA 16802, USA

[2]Department of Mathematics, Washington State University, Pullman, WA 99164, USA
berlyand@math.psu.edu; panchenko@math.wsu.edu

(Received 12 July 2005 and in revised form 29 June 2006)

We study the overall dissipation rate of highly concentrated non-colloidal suspensions of rigid neutrally buoyant particles in a Newtonian fluid. This suspension is confined to a finite size container, subject to shear or extensional boundary conditions at the walls of the container. The corresponding dissipation rates determine the effective shear viscosity $\mu^\star$ and the extensional effective viscosity $\lambda^\star$. We use recently developed discrete network approximation techniques to obtain discrete forms for the overall dissipation rates, and analyse their asymptotics in the limit when the characteristic interparticle distance goes to zero. The focus is on the finite size and particle wall effects in spatially disordered arrays. Use of the network approximation allows us to study the dependence of $\mu^\star$ and $\lambda^\star$ on variable distances between neighbouring particles in such arrays.

Our analysis, carried out for a two-dimensional model, can be characterized as global because it goes beyond the local analysis of flow in a single gap between two particles and takes into account hydrodynamic interactions in the entire particle array. The principal conclusion in the paper is that, in general, asymptotic formulae for $\mu^\star$ and $\lambda^\star$ obtained by global analysis are different from the formulae obtained from local analysis. In particular, we show that the leading term in the asymptotics of $\mu^\star$ is of lower order than suggested by the local analysis (weak blow-up), while the order of the leading term in the asymptotics of $\lambda^\star$ depends on the geometry of the particle array (either weak or strong blow-up). We obtain geometric conditions on a random particle array under which the asymptotic order of $\lambda^\star$ coincides with the order of the local dissipation in a gap between two neighbouring particles, and show that these conditions are generic. We also provide an example of a uniformly closely packed particle array for which the leading term in the asymptotics of $\lambda^\star$ degenerates (weak blow-up).

1. Introduction

Concentrated suspensions are important in many industrial applications such as drilling, transport of water-coal slurries, food processing, cosmetics and ceramics manufacture. In nature, flows of concentrated suspensions appear as mud slides, lava flows and soils liquefied by earthquake-induced vibrations (Shook & Roco 1991; Carreau & Cotton 2002; Coussot 2002). An evaluation of the effective viscosity of such suspensions is a key issue for both theory and practical applications.

An asymptotic formula for the effective viscosity of a suspension of non-colloidal particles in a Newtonian fluid, derived by Frankel & Acrivos (1967), is based on the

local lubrication analysis of the energy dissipation rate in the narrow gap between a pair of nearly touching particles. The distance between two neighbouring particles in a periodic array is the small parameter in the problem. For periodic arrays, this interparticle distance is uniquely determined by the volume fraction of particles, so that the asymptotics of the effective viscosity is obtained as a function of the volume fraction ϕ that is close to the maximal packing volume fraction ϕ_{rcp}. The asymptotics of the effective viscosity obtained by Frankel & Acrivos (1967) has the form

$$A\epsilon^{-1} + O(\ln \epsilon^{-1}), \tag{1.1}$$

as $\epsilon \to 0$, where $\epsilon = 1 - (\phi/\phi_{rcp})^{1/3}$. The formulae for effective viscosity of periodic suspensions in the whole space $\boldsymbol{R}^3$ (without boundary) subject to a prescribed linear flow, obtained by Nunan & Keller (1984), also rely on the local lubrication analysis. Asymptotic representations for the components of the effective viscosity tensor calculated by Nunan & Keller (1984) are of the form

$$A\epsilon^{-1} + B \ln \epsilon^{-1} + O(1), \tag{1.2}$$

where the leading term is, roughly speaking, generated by the local squeezing flows in the lubrication gaps between the particles, while all other types of local motion can contribute only to the second term. Concentrated random suspensions have been investigated numerically by Sierou & Brady (2001, 2002) using accelerated Stokesian dynamics. It was observed that the behaviour of the effective high-frequency dynamic shear viscosity of disordered suspensions can be accurately described by the asymptotic $B \ln \epsilon^{-1}$, indicating degeneration of the leading term in the asymptotic expansions (1.2) (weak blow-up). This suggests that for generic random suspensions, the asymptotics of the effective viscosity defined by the (properly normalized) global dissipation rate cannot be identified with the local dissipation rate in a single gap.

Finally, there is a large body of literature on colloidal suspensions. Since in this paper we restrict our attention to non-colloidal suspensions (particles are large enough so that Brownian forces can be neglected), we only mention the papers by Ball & Melrose (1997*a*, *b*) in which a computational method for concentrated colloidal suspensions was developed. Their approach has some similarities to ours, in particular in the use of Delaunay triangulation and lubrication approximation for local squeeze flows between neighbouring particles. However, the main issue in these papers is the reduction of computational complexity in terms of the total number of particles, whereas we use network theory for analysis of viscous dissipation rates.

Specifically, in this paper we use the discrete network approximation of the dissipation rate proposed in Berlyand, Borcea & Panchenko (2005*a*) to study the asymptotics of the shear effective viscosity $\mu^\star$ and the extensional effective viscosity $\lambda^\star$ corresponding to general disordered particle arrays of finite size. For such arrays, the volume fraction alone is not sufficient for determining the effective viscosity. In particular, from the analysis presented in this paper it follows that the values of $\lambda^\star$ may be dramatically different for arrays with the same volume fraction, but with a different geometric distribution of particles. Therefore, instead of ϵ, we use the interparticle distances δ_{ij} between the neighbouring particles. These distances are supposed to have the same order of magnitude δ.

The discrete dissipation rate of Berlyand *et al.* (2005*a*) accounts for the long-range hydrodynamic interactions between the particles, and provides an algorithm for calculation of the effective viscosity, which takes into account variable distances between neighbouring particles in non-periodic arrays. Furthermore, Berlyand *et al.* (2005*a*) observed that the leading term of the asymptotics may degenerate owing to

the external boundary conditions and geometry of the particle array, whereas in the scalar case (Berlyand & Kolpakov 2001) the order of the leading term is the same for all particle arrays that form a connected network. This paper is devoted to a detailed study of this degeneration phenomenon. In particular, we clarify the issue of weak versus strong blow-up in the asymptotics of the effective viscosity.

The emphasis in this paper is on the finite size effects and role of the particle–wall interactions (boundary conditions). Although our analysis is aimed at understanding three-dimensional suspensions, we use a two-dimensional model for technical simplicity. This model captures qualitative effects of weak and strong blow-up, and at the same time it is amenable to a relatively simple mathematical analysis. We remark here that two-dimensional models may have special features which have no analogue in three dimensions. In this paper, we do not consider these features (see § 3.4, Appendix B, and Berlyand *et al.* 2005*b* for more details).

We consider a suspension confined to a finite box Ω of side length $L = 2$. The particle radius a is small compared to L, and the number of particles N is close to the maximal packing number which is finite for given a and Ω. In our study, a is fixed, and therefore we do not pass to the classical homogenization limit $a \to 0$, $N \to \infty$, in which the effects due to the particle–wall interactions (or, equivalently, prescribed boundary conditions) may vanish. Therefore, our approach is different from the homogenization-based procedures and our definitions of the effective viscosities are more directly linked to the viscometric measurements, since they take into account particle–wall and finite size effects. This seems to be in agreement with Sierou & Brady (2002), where the notion of the universal viscosity which does not depend on the size of the apparatus and particle–wall interactions is characterized as "questionable". The importance of the finite size effects is demonstrated in the paper. Indeed, we show that the asymptotic order of the effective viscosities is determined by the interplay between boundary velocities and the geometry of the particle array. In particular, the leading term in the asymptotics of the shear viscosity $\mu^\star$ is always degenerate (weak blow-up), while local analysis alone predicts no degeneration (strong blow-up). The asymptotic order of the extensional viscosity $\lambda^\star$ depends on the geometry of the particle array. We prove that for generic arrays, the leading-order term of $\lambda^\star$ does not degenerate. This non-degeneration is linked to the percolation of the local squeezing flows in the lubrication gaps. Thus, for a generic array, $\mu^\star$ and $\lambda^\star$ have vastly different values, and their ratio depends on the typical interparticle distance. In the paper, $\mu^\star$ is defined via the off-diagonal component of the effective stress, while the definition of $\lambda^\star$ involves the effective normal stress difference (see (2.14), (2.17) below). Therefore, our results suggest that the diagonal and off-diagonal components of the effective stress have different asymptotic scalings. The same conclusion was reached by Sierou & Brady (2002) who investigated effective stress in shear flow by means of numerical simulations using accelerated Stokesian dynamics.

2. From continuum to discrete dissipation rate. Network approximation

2.1. *Mathematical model*

We consider a non-colloidal concentrated suspension of rigid neutrally buoyant particles in a viscous incompressible Newtonian fluid. The quasi-static fluid flow at low Reynolds number is governed by Stokes equations

$$\mu \Delta \boldsymbol{v} - \nabla P = 0, \quad \text{div } \boldsymbol{v} = 0 \quad \text{in } \Omega_F. \tag{2.1}$$

where μ is the fluid viscosity, $\boldsymbol{v}$ the velocity field, and P is the pressure.

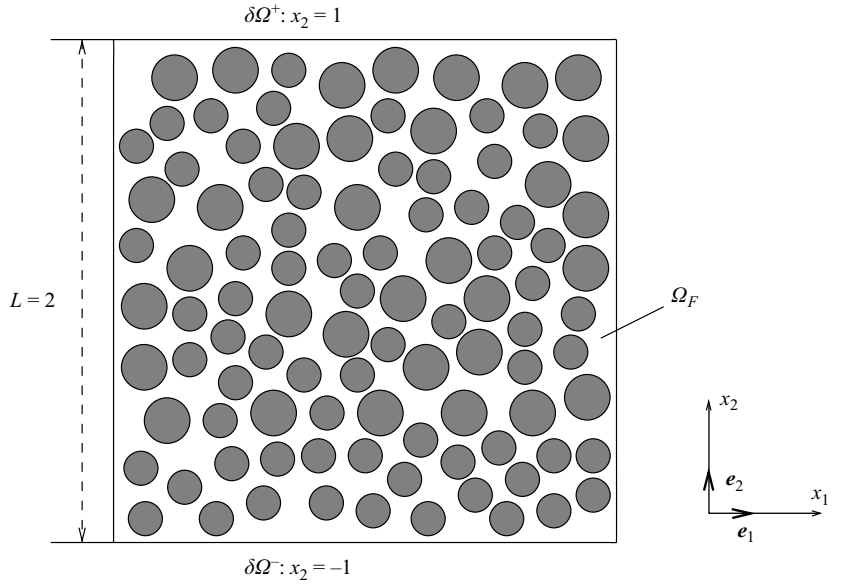

FIGURE 1. A concentrated suspension in a domain Ω.

The suspension is confined to a square box Ω of side length $L = 2$. The part of Ω which is not occupied by the particles is the fluid domain, denoted by Ω_F. The boundary of Ω is denoted by $\partial\Omega$. The upper and lower sides of $\partial\Omega$ are denoted by $\partial\Omega^+ = \{\boldsymbol{x} : x_2 = 1\}$ and $\partial\Omega^- = \{\boldsymbol{x} : x_2 = -1\}$, respectively. We also let $\boldsymbol{e}_1, \boldsymbol{e}_2$ denote the Cartesian basis vectors parallel to the sides of $\partial\Omega$ (see figure 1). The particles D^j, $j = 1, 2, \ldots, N$ are modelled as rigid disks with centres $\boldsymbol{x}^j$, placed in Ω.

We study shear and extensional boundary conditions applied on $\partial\Omega^+$, $\partial\Omega^-$ (upper and lower walls of the apparatus) (Schowalter 1978). The shear type boundary conditions are given by

$$\boldsymbol{v}_{|\partial\Omega} \equiv \boldsymbol{g} = \begin{pmatrix} \frac{1}{2}\gamma L \\ 0 \end{pmatrix} \text{ on } \partial\Omega^+, \qquad \boldsymbol{v}_{|\partial\Omega} \equiv \boldsymbol{g} = \begin{pmatrix} -\frac{1}{2}\gamma L \\ 0 \end{pmatrix} \text{ on } \partial\Omega^-, \tag{2.2}$$

where γ is the shear rate. These boundary conditions are obtained by restricting the shear flow velocity

$$\boldsymbol{v}^0_{sh} = \begin{pmatrix} \gamma x_2 \\ 0 \end{pmatrix} \tag{2.3}$$

to the upper ($\partial\Omega^+$) and lower ($\partial\Omega^-$) parts of $\partial\Omega$. Similarly, for extensional flows, the extension rate is ε (note the difference in notation from ϵ employed in § 1), and the boundary conditions are obtained by restricting the velocity field

$$\boldsymbol{v}^0_{ext} = \begin{pmatrix} \varepsilon x_1 \\ -\varepsilon x_2 \end{pmatrix} \tag{2.4}$$

to $\partial\Omega^{\pm}$, which results in

$$\boldsymbol{g} = \begin{pmatrix} \varepsilon x_1 \\ -\frac{1}{2}\varepsilon L \end{pmatrix} \text{ on } \partial\Omega^+, \qquad \boldsymbol{g} = \begin{pmatrix} \varepsilon x_1 \\ \frac{1}{2}\varepsilon L \end{pmatrix} \text{ on } \partial\Omega^-. \tag{2.5}$$

The lateral part of the boundary is supposed to be traction-free.

To define particle velocities, we first recall that a rigid body moving in the plane with the basis $\boldsymbol{e}_1, \boldsymbol{e}_2$ has a velocity vector of the form

$$\boldsymbol{v}^j(\boldsymbol{x}) = \boldsymbol{T}^j + \omega^j \boldsymbol{e}_3 \times (\boldsymbol{x} - \boldsymbol{x}^j), \quad \boldsymbol{x} \in D^j, \tag{2.6}$$

where $\boldsymbol{T}^j, \omega^j$ are translational and angular velocities, respectively. In (2.6), $\boldsymbol{e}_3$ is the unit vector perpendicular to the plane of motion. Both $\boldsymbol{T}^j$ and ω^j are unknown and must be determined in the course of solving the problem, together with the fluid velocity and pressure. Each particle D^j moves with the velocity (2.6) from its original equilibrium position to a new equilibrium position after the external boundary conditions are applied. Since the particles are neutrally buoyant, and each rigid disk is in equilibrium, the total force and torque exerted on D^j by the fluid must be zero, which provides the boundary conditions on the particle boundaries ∂D^j:

$$\int_{\partial D^j} \boldsymbol{S}\boldsymbol{n}^j \, \mathrm{d}s = \boldsymbol{0}, \qquad \int_{\partial D^j} \boldsymbol{n}^j \times \boldsymbol{S}\boldsymbol{n}^{(j)} \, \mathrm{d}s = \boldsymbol{0}, \text{ for } j = 1, 2, \ldots, N, \tag{2.7}$$

where $\boldsymbol{n}^j$ is the exterior unit normal to ∂D^j, and

$$\boldsymbol{S} = 2\mu \boldsymbol{e}(\boldsymbol{v}) - P\boldsymbol{I}. \tag{2.8}$$

In (2.8) and throughout the paper, $\boldsymbol{e}(\boldsymbol{v})$ denotes the strain rate tensor defined by

$$\boldsymbol{e}(\boldsymbol{v}) = \tfrac{1}{2}(\nabla \boldsymbol{v} + (\nabla \boldsymbol{v})^T), \tag{2.9}$$

the superscript T stands for the transposed tensor, and $\boldsymbol{I}$ denotes the unit tensor.

The problem of finding the fluid velocity satisfying the boundary conditions (2.6), (2.7) can be cast in the variational form (see, e.g. Kim & Karilla 1991, § 2.2.2). The actual fluid flow velocity minimizes the dissipation rate functional

$$W_{\Omega_F}(\boldsymbol{u}) = 2\int_{\Omega_F} e(\boldsymbol{u})_{ij} e(\boldsymbol{u})_{ij} \, \mathrm{d}\boldsymbol{x}, \tag{2.10}$$

over all admissible velocity fields $\boldsymbol{u}$. An admissible velocity field lies in a class $\mathscr{U}$ of appropriately smooth divergence-free trial vector functions that satisfy the prescribed boundary conditions on the external boundary and the conditions (2.6) on the particle boundaries. We also recall that conditions (2.7) are known in calculus of variations as natural boundary conditions, which means that the trial functions need not satisfy these conditions, but the minimizer (the actual fluid velocity field) should satisfy them.

Equation (2.10) means, in particular, that the energy dissipation rate E in the fluid is the minimal value of W_{Ω_F}, attained when the trial field $\boldsymbol{u}$ is the actual velocity filed $\boldsymbol{v}$. Concisely,

$$E = W_{\Omega_F}(\boldsymbol{v}) = \min_{\boldsymbol{u} \in \mathscr{U}} W_{\Omega_F}(\boldsymbol{u}). \tag{2.11}$$

Equation (2.11) is important, since calculation of the effective viscosities essentially amounts to calculation of E, as seen in the next section. Also, note that any trial function $\boldsymbol{u}$ from $\mathscr{U}$ provides an upper bound for E, namely $E \leqslant W_{\Omega_F}(\boldsymbol{u})$.

2.2. *Effective shear and extensional viscosities*

2.2.1. *Effective dissipation rates*

We assume that the suspension can be modelled on a macroscale by a single-phase fluid, called an *effective fluid*. This assumption is consistent with most of the numerical and experimental studies of effective viscosity ranging from the dilute limit to high

concentration (Einstein 1906*a*, *b*; Frankel & Acrivos 1967; Batchelor & Green 1972; Kim & Karilla 1991).

The velocity field of the effective fluid is denoted by $\boldsymbol{v}^0$. The effective fluid is subject to the same external boundary conditions as the flow of the suspension.

In this paper, we do not derive or postulate the precise from of the constitutive law for the effective fluid. For our purposes, it is sufficient to assume simply that the effective stress tensor $\boldsymbol{S}^0$ is constant whenever the effective strain rate $\boldsymbol{e}(\boldsymbol{v}^0)$ is constant (in other words, the effective fluid is homogeneous). The possible constitutive relations are explored indirectly, by using the fundamental principle (Einstein 1906*a*, *b*), that the viscous energy dissipation rate of the suspension must be equal to the dissipation rate of the effective homogeneous fluid. The dissipation rates are defined by

$$E = \int_{\Omega_F} \boldsymbol{S} \cdot \boldsymbol{e}(\boldsymbol{v})\,\mathrm{d}\boldsymbol{x} = 2\mu \int_{\Omega_F} \boldsymbol{e}(\boldsymbol{v}) \cdot \boldsymbol{e}(\boldsymbol{v})\,\mathrm{d}\boldsymbol{x} \tag{2.12}$$

in the suspension, and

$$E^0 = \int_{\Omega} \boldsymbol{S}^0 \cdot \boldsymbol{e}(\boldsymbol{v}^0)\,\mathrm{d}\boldsymbol{x}, \tag{2.13}$$

in the effective fluid. In the equations (2.12), (2.13), $\boldsymbol{S} \cdot \boldsymbol{e} = \boldsymbol{S}_{ij}\boldsymbol{e}_{ij}$ is the inner product of tensors.

For small particle volume fractions, (Einstein 1906*a*, *b*; Batchelor & Green 1972), this principle was further combined with the assumption that the effective fluid is Newtonian with a constant effective viscosity. However, for concentrated suspensions this assumption is not validated by a rigorous mathematical derivation or experimental measurements, and at present the question of finding the effective constitutive law for such suspensions is still open. Theoretical studies by Brady & Morris (1997) have shown that the high-Péclet number limit (when the Brownian forces are much weaker than hydrodynamic forces) is singular and produces non-Newtonian behaviour. Our calculations of the effective viscosity also suggest non-Newtonian behaviour for irregular (non-periodic or random) suspensions in containers of finite size.

We use the rheological definitions of shear and extensional viscosities as ratios of the corresponding components of the stress and strain rate tensors. To calculate the asymptotics of the two viscosities, we employ the network approximation introduced in (Berlyand *et al.* 2005*a*). We analyse the network functional (discrete dissipation rate) introduced in Berlyand *et al.* (2005*a*) and show that the standard relation between two viscosities which holds for Newtonian fluids (see, chap. 9 Schowalter 1978 for the three-dimensional case and Appendix A for two-dimensional case) does not hold. Indeed, we show that for generic disordered arrays, the ratio of the two effective viscosities blows up as the reciprocal of the typical interparticle distance. This suggests different asymptotic scaling for components of the effective stress tensor and is therefore an indicator of the non-Newtonian behaviour, detected numerically in Sierou & Brady (2002) (see also Stickel & Powell (2005) for a discussion of non-Newtonian rheology of concentrated suspensions).

Finally, in this paper we are concerned with the instantaneous effective viscosity, and therefore we do not consider the evolution problem. However, we study arbitrary arrays of particles, which makes it possible to extend our analysis to evolution of microstructure problems. Clearly, analysis of the instantaneous response for arbitrary arrays is an unavoidable step in understanding of the evolution problem.

2.2.2. *Shear viscosity*

Suppose that a homogeneous effective fluid undergoes a steady shear flow with the shear rate γ. The velocity field $\boldsymbol{v}_{sh}$ satisfies the shear type boundary conditions (2.2). The effective shear viscosity is defined by (see (A 2))

$$\mu^\star = \frac{S^0_{12}}{\gamma} = 2\frac{E^0}{\gamma^2|\Omega|}, \tag{2.14}$$

where S^0_{12} is the corresponding component of the effective stress tensor and $|\Omega| = \int_\Omega \mathrm{d}\boldsymbol{x}$. Since $E = E^0$, the equivalent definition is

$$\mu^\star = 2E\gamma^{-2}|\Omega|^{-1} = 4\mu\gamma^{-2}|\Omega|^{-1}\int_{\Omega_F} \boldsymbol{e}(\boldsymbol{v}_{sh})\cdot\boldsymbol{e}(\boldsymbol{v}_{sh})\,\mathrm{d}\boldsymbol{x}. \tag{2.15}$$

Thus the calculation of $\mu^\star$ amounts to evaluation of the total dissipation rate integral

$$E_{sh} = 2\mu\int_{\Omega_F} \boldsymbol{e}(\boldsymbol{v}_{sh})\cdot\boldsymbol{e}(\boldsymbol{v}_{sh})\,\mathrm{d}\boldsymbol{x}, \tag{2.16}$$

where $\boldsymbol{v}_{sh}$ solves (2.1)–(2.7).

2.2.3. *Extensional viscosity*

A steady extensional flow of the effective fluid is characterized by a constant extension rate ε. The velocity $\boldsymbol{v}^0_{ext}$ satisfies the extensional boundary conditions (2.5). The extensional viscosity (see, e.g. Schowalter 1978, chap. 9) may be defined by

$$\lambda^\star = \frac{S^0_{11} - S^0_{22}}{\varepsilon}, \tag{2.17}$$

where S^0_{11}, S^0_{22} are components of the effective stress tensor. Since $E^0 = \int_\Omega \boldsymbol{S}^0\cdot\boldsymbol{e}(\boldsymbol{v})^0_{ext}\,\mathrm{d}\boldsymbol{x} = (S^0_{11} - S^0_{22})\varepsilon|\Omega|$, the effective extensional viscosity can be defined in terms of the suspension dissipation rate E, as follows.

$$\lambda^\star = \frac{E}{\varepsilon^2|\Omega|} = 2\mu\varepsilon^{-2}|\Omega|^{-1}\int_{\Omega_F} \boldsymbol{e}(\boldsymbol{v}_{ext})\cdot\boldsymbol{e}(\boldsymbol{v}_{ext})\,\mathrm{d}\boldsymbol{x}, \tag{2.18}$$

and calculation of $\lambda^\star$ again reduces to evaluation of the total dissipation rate (2.16) with $\boldsymbol{v}_{sh}$ replaced by $\boldsymbol{v}_{ext}$. In the remaining part of the paper we derive asymptotic formulae for the total dissipation rate under shear and extensional boundary conditions.

2.3. *Discrete network*

Let us consider an arbitrary distribution of circular particles (disks) D^i of radius a. The particle centres are points $\boldsymbol{x}^i$, $i = 1, 2, \ldots, N$. We consider the case when N is close to the maximal close-packing number, which is finite and independent of δ. We are interested in a high concentration regime when neighbouring particles are close to touching. Note that while for a periodic array the notion of a neighbouring particle is obvious, for disordered arrays it is not immediate. We introduce it via a Voronoi tessellation (Edelsbrunner 2000). The central notion here is that of a Voronoi cell V_i which is a polygon that consists of all points in the plane which are closer to $\boldsymbol{x}^i$ than to any other particle centre $\boldsymbol{x}^j$, $j \neq i$. Each Voronoi cell contains only one particle centre, and different Voronoi cells do not overlap. Together, Voronoi cells form a partition of Ω.

DEFINITION 2.1. *We call particles D^j, D^i* neighbours *if their centres $\boldsymbol{x}^i$ and $\boldsymbol{x}^j$ have a common edge in the Voronoi tessellation, that is, the corresponding Voronoi polygons*

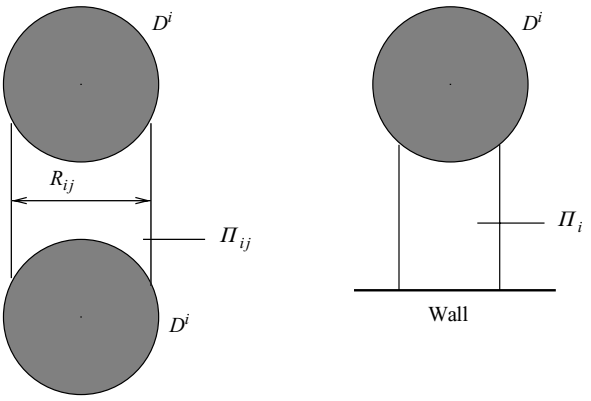

FIGURE 2. An interparticle gap Π_{ij} between D^i and D^j and a particle–wall gap Π_i.

V_i and V_j share an edge. Furthermore, we call a particle D^i adjacent to the boundary *if the corresponding Voronoi cell has an edge that belongs either to upper ($\partial\Omega^+$) or lower ($\partial\Omega^-$) portions of the boundary of Ω. For each $i = 1, 2, \ldots, N$, define the index sets $\mathcal{N}_i$, I by*

$$\mathcal{N}_i = \{j \in \{1, 2, \ldots, N\},\ j \neq i,\ \textit{such that } D^j \textit{ is a neighbour of } D^i\}, \tag{2.19}$$

$$I = \{i \in \{1, 2, \ldots, N\} \textit{ such that } D^i \textit{ is adjacent to the boundary}\}. \tag{2.20}$$

The minimal distance between neighbouring particles D^i and D^j is given by

$$\delta_{ij} = |\boldsymbol{x}^i - \boldsymbol{x}^j| - 2a. \tag{2.21}$$

We call δ_{ij} *interparticle distances*. If a disk D^i is adjacent to the boundary, we define the particle–wall minimal distance δ_i by

$$\delta^i = \operatorname{dist}(\boldsymbol{x}^i, \partial\Omega) - a. \tag{2.22}$$

To model the high-concentration regime, we assume that δ_{ij} and δ_i satisfy

$$\delta_{ij} = \delta d_{ij}, \qquad \delta_i = \delta d_i, \tag{2.23}$$

where $\delta \ll 1$ is a small non-dimensional parameter in the problem, and the *scaled* (*by* δ) *interparticle distances* d_{ij}, d_i satisfy

$$0 < c \leqslant d_{ij} \leqslant 1, \quad c \leqslant d_i \leqslant 1, \tag{2.24}$$

with an absolute constant c independent of i, j. The inequality (2.24) describes the case when neighbouring particles are close to each other but do not touch.

For each pair of neighbouring particles D^i and D^j, we introduce an interior lubrication gap Π_{ij} which represents a narrow fluid region where lubrication effects are very strong, as shown on figure 2. The orientation of each interior gap Π_{ij} relative to a disk D^i is specified by a unit vector

$$\boldsymbol{q}^{ij} = \frac{\boldsymbol{x}^i - \boldsymbol{x}^j}{|\boldsymbol{x}^i - \boldsymbol{x}^j|}. \tag{2.25}$$

We also let $\boldsymbol{p}^{ij}$ be the unit vector obtained by rotating $\boldsymbol{q}^{ij}$ clockwise by $\pi/2$ (see figure 3). For each particle D^i adjacent to the boundary, we introduce a particle wall lubrication gap Π_i. These gaps are always oriented perpendicular to the wall, which

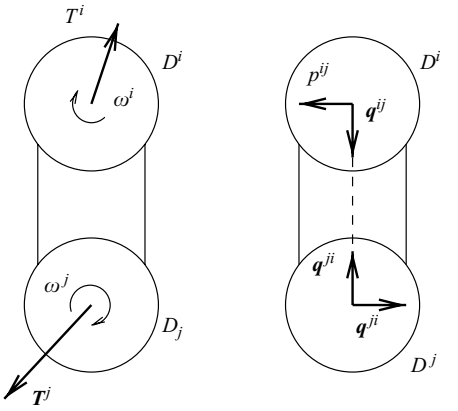

FIGURE 3. Assignment of $\boldsymbol{T}^i, \omega^i$ and orientation of the gap between two neighbouring particles.

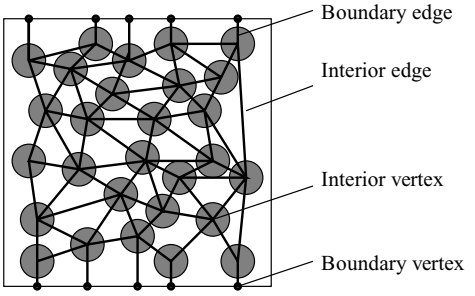

FIGURE 4. The suspension and the corresponding network.

means that the orientation vectors $\boldsymbol{q}^i$ are vertical, while $\boldsymbol{p}^i$ are horizontal. This reflects the physical fact that the zone of the largest energy dissipation is located near the shortest line connecting $\boldsymbol{x}^i$ with the boundary. The vectors $\boldsymbol{q}^i$ always point away from D^i toward the wall. Therefore, $\boldsymbol{q}^i = \boldsymbol{e}_2$, (respectively, $-\boldsymbol{e}_2$), when D^i is adjacent to $\partial\Omega^+$ (respectively, $\partial\Omega^-$).

The network denoted by Γ is a graph (a set of vertices connected by edges) corresponding to the particle array together with the interior and particle–wall lubrication gaps. The centres of the particles $\boldsymbol{x}^i$ are called the interior vertices of the network, and the lubrication gaps are represented by the edges connecting either two neighbouring vertices (interior edges), or a vertex and the wall (boundary edges). The points of intersection of boundary edges with the boundary are called boundary vertices. These are also included into the network (see figure 4).

Note that Γ is essentially the Delaunay graph (Edelsbrunner 2000) dual to the Voronoi tessellation, and the above notions admit straightforward generalization to three dimensions.

2.4. *Discrete dissipation form. Approximation of the dissipation rate and effective viscosities*

To define the network approximation, we first assign a translational velocity $\boldsymbol{T}^i$ and an angular velocity ω^i of a particle D^i to the corresponding interior vertex $\boldsymbol{x}^i$. At the boundary vertices, we prescribe the velocity vector $\boldsymbol{g}$ which represents the boundary conditions (either shear or extensional). Next, to each edge of the network

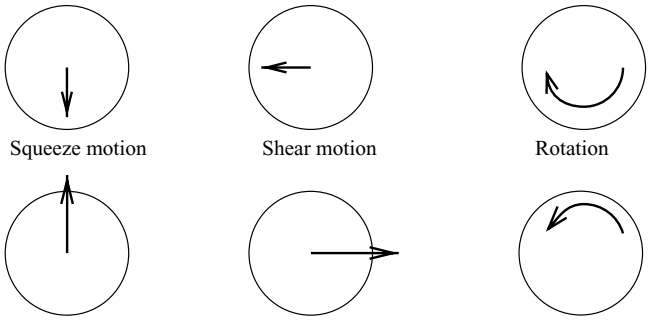

FIGURE 5. Three elementary motions. Arrows represent the boundary conditions.

we associate a dissipation rate W^{ij} (W^i), calculated in the corresponding gap Π_{ij} (Π_i). The calculation of the dissipation rates employs lubrication approximation in the gap. The velocity in the gap is decomposed into three velocities, representing the 'elementary' motions called squeeze motion, shear and rotation (see figure 5). The total velocity field in a gap is the sum of these elementary velocities and a residual velocity field, whose contribution to the gap dissipation rate is $O(1)$ as $\delta \to 0$. Lubrication approximations for each of the elementary velocities and estimates for the residual can be found in Berlyand *et al.* (2005*a*).

Using approximations of the elementary velocities to calculate (up to the terms of order $O(1)$ as $\delta \to 0$) the dissipation rates in each gap we obtain

$$W^{ij} = \delta^{-3/2} C^{ij}_{sp} [(\boldsymbol{T}^i - \boldsymbol{T}^j) \cdot \boldsymbol{q}^{ij}]^2 + \delta^{-1/2} C^{ij}_{sh} [(\boldsymbol{T}^i - \boldsymbol{T}^j) \cdot \boldsymbol{p}^{ij} + a\omega^i + a\omega^j]^2 + \delta^{-1/2} C^{ij}_{rot} a^2 (\omega^i - \omega^j)^2, \quad (2.26)$$

in the interior gaps Π_{ij}, and

$$W^i = \delta^{-3/2} C^i_{sp} [(\boldsymbol{T}^i - \boldsymbol{g}) \cdot \boldsymbol{q}^i]^2 + \delta^{-1/2} C^i_{rot} a^2 (2\omega^i)^2 + \delta^{-1/2} C^i_{sh} [(\boldsymbol{T}^i - \boldsymbol{g}) \cdot \boldsymbol{p}^i + a\omega^i]^2 \quad (2.27)$$

in the particle–wall gaps Π_i. The expressions for factors C^{ij}_{sp}, C^{ij}_{sh}, C^{ij}_{rot} and C^i_{sp}, C^i_{sh}, C^i_{rot} are calculated explicitly in Berlyand *et al.* (2005*a*):

$$\left.\begin{aligned} C^{ij}_{sp} &= \tfrac{3}{4}\pi\mu \left(\frac{a}{d_{ij}}\right)^{3/2} + \frac{27}{10}\pi\mu \left(\frac{a}{d_{ij}}\right)^{1/2}, & C^i_{sp} &= \tfrac{3}{4}\pi\mu \left(\frac{a}{d_i}\right)^{3/2} + \frac{27}{10}\pi\mu \left(\frac{a}{d_i}\right)^{1/2}, \\ C^{ij}_{sh} &= \tfrac{1}{2}\pi\mu \left(\frac{a}{d_{ij}}\right)^{1/2}, & C^i_{sh} &= \tfrac{1}{2}\pi\mu \left(\frac{a}{d_i}\right)^{1/2}, \\ C^{ij}_{rot} &= \tfrac{9}{16}\pi\mu \left(\frac{a}{d_{ij}}\right)^{1/2}. & C^i_{rot} &= \tfrac{9}{16}\pi\mu \left(\frac{a}{d_i}\right)^{1/2}. \end{aligned}\right\} \quad (2.28)$$

In the formula (2.28), d_{ij}, d_i are the scaled interparticle distances defined in (2.24).

The sum of the local dissipation rates W^{ij}, W^i is a quadratic form $Q = \sum_{\Pi_{ij}} W^{ij} + \sum_{\Pi_i} W^i$ on the unknown translational velocities $\boldsymbol{T}^i$ and angular velocities ω^i of the particles D^i. It also depends on the prescribed velocity $\boldsymbol{g}$ of the walls via the terms W^i.

The form Q is the called the *discrete dissipation form*. It provides an approximation for the continuum dissipation rate functional W_{Ω_F} in the variational principle (2.10). An explicit expression for Q is presented in Appendix B, equation (B 1).

The main idea of the network approximation is that most of the energy is dissipated in the gaps Π_{ij}, Π_i, so that the exact dissipation rate E (the minimum of W_{Ω_F}) is approximately equal to the discrete dissipation rate E_d which is the minimum of Q:

$$\min W_{\Omega_F} \equiv E = E_d + O(1) \equiv \min Q + O(1) \quad \text{as } \delta \to 0. \tag{2.29}$$

Here, $O(1)$ denotes quantities which are bounded by a constant as δ goes to zero. Since in this limit E_d blows up, $O(1)$ represents a small discrepancy between the actual dissipation rate and its discrete approximation. The minimum of Q is taken over all possible collections of particle velocities $\boldsymbol{T}^i, \omega^i$. This is not surprising, since the trial functions in the admissible class $\mathscr{U}$ for the continuum dissipation functional W_{Ω_F} may have arbitrary translational and angular velocities on the particles. The continuum problem is constrained by the prescribed external boundary conditions. In the discrete approximation, the boundary conditions $\boldsymbol{g}$ are explicitly incorporated into the formula for Q via (2.27).

3. Analysis of the discrete dissipation rate

3.1. *Truncation of the discrete dissipation functional and overview of the related computational issues*

The two major factors that determine asymptotic behaviour of the discrete dissipation form Q are geometry of the network and the nature of the boundary conditions. The objective of this section is to analyse in detail the role of both of these factors. Separating terms of different orders in δ, we decompose the form Q as follows.

$$Q = \delta^{-3/2}\widehat{Q} + \delta^{-1/2}Q', \tag{3.1}$$

where the coefficients of the forms $\widehat{Q}$ and Q' do not depend on δ. For future reference, we give the explicit equation for $\widehat{Q}$:

$$\widehat{Q} = \frac{1}{2}\sum_{i=1}^{N}\sum_{j\in\mathscr{N}_i} C_{sp}^{ij}[(\boldsymbol{T}^i - \boldsymbol{T}^j)\cdot\boldsymbol{q}^{ij}]^2 + \sum_{i\in I} C_{sp}^{i}[(\boldsymbol{T}^i - \boldsymbol{g})\cdot\boldsymbol{q}^{i}]^2, \tag{3.2}$$

where the second summation is taken over all vertices adjacent to the boundary. Note that $\widehat{Q}$ depends only on translational velocities due to squeezing motions, while the contributions from other types of local motions (both angular and translational velocities) are absorbed into Q'. Since the functional $\widehat{Q}$ is simpler than Q, we want to estimate the discrete dissipation rate E_d (the minimum of Q) in terms of the minimum of $\widehat{Q}$. The obvious problem here is that the collection of velocities that minimizes Q would not necessarily minimize $\widehat{Q}$ and vica versa. To clarify this issue, denote the minimal value of $\widehat{Q}$ by $\widehat{E}$, and suppose that this minimal value is attained for the (δ-independent) translational velocities $\widehat{\boldsymbol{T}^i}$. Furthermore, we denote by $\boldsymbol{T}^i_{min}, \omega^i_{min}$ the translational and angular velocities minimizing the complete functional Q. Then we can write

$$\begin{aligned}\delta^{-3/2}\widehat{E} \equiv \delta^{-3/2}\widehat{Q}(\widehat{\boldsymbol{T}^i}) \leqslant \delta^{-3/2}\widehat{Q}\big(\boldsymbol{T}^i_{min}, \omega^i_{min}\big) \leqslant E_d \\ \equiv Q\big(\boldsymbol{T}^i_{min}, \omega^i_{min}\big) \leqslant \delta^{-3/2}\widehat{Q}(\widehat{\boldsymbol{T}^i}) + \delta^{-1/2}Q'(\widehat{\boldsymbol{T}}^1, \ldots, \widehat{\boldsymbol{T}}^N, \boldsymbol{\omega}^1 = \boldsymbol{\omega}^2 = \ldots = \boldsymbol{\omega}^N = 0).\end{aligned} \tag{3.3}$$

The first inequality is true since $\boldsymbol{T}^i_{min}, \omega^i_{min}$ is not in general a minimizer for $\widehat{Q}$, so inserting them into $\widehat{Q}$ produces the value that is larger than $\widehat{E}$. The second inequality is true because $\delta^{-3/2}\widehat{Q}$ is a part of Q, and the difference $Q - \delta^{-3/2}\widehat{Q} = \delta^{-1/2}Q'$, is a

sum of squares and is therefore non-negative. Finally, the last inequality holds because the collection $\boldsymbol{T}^i = \widehat{\boldsymbol{T}}^i, \omega^i = 0, i = 1, \ldots, N$, corresponding to purely translational flow of particles, is an admissible trial velocity field, but not necessarily the actual collection of velocities minimizing Q.

Since coefficients of Q' are δ-independent, and the minimizing collection for $\widehat{Q}$ is also independent of δ, $\delta^{-1/2}Q'(\widehat{\boldsymbol{T}}^i, \omega^i = 0) = O(\delta^{-1/2})$, and (3.3) yields $\delta^{-3/2}\widehat{E} \leqslant E_d \leqslant \delta^{-3/2}\widehat{E} + O(\delta^{-1/2})$, and thus

$$E_d = \delta^{-3/2}\widehat{E} + O(\delta^{-1/2}) \quad \text{as } \delta \to 0, \tag{3.4}$$

Equation (3.4) enables us to calculate the leading term in the asymptotics of the effective viscosity by solving a simplified minimization problem involving only the translational particle velocities (rotations are neglected). To the leading order in δ, the effective viscosities are determined by the discrete dissipation rate $\delta^{-3/2}\widehat{E}$ where $\widehat{E}$ is the minimum of $\widehat{Q}$. However, this algorithm is useful only when

$$\widehat{E} > 0, \tag{3.5}$$

because, in this case, the leading term in the asymptotics of the dissipation rate is of order $\delta^{-3/2}$. We shall call this situation the *strong blow-up*. If $\min \widehat{Q} = 0$, the leading term degenerates, and the rate of blow-up of E_d is at most $\delta^{-1/2}$ (the *weak blow-up*). When weak blow-up occurs, the full form Q has to be minimized to obtain the asymptotics of the effective viscosity. The simple but important observation here is that for the shear boundary conditions, the leading term is always degenerate. To explain this, consider dependence of $\widehat{Q}$ on the boundary conditions. The second sum in (3.2) represents the contribution of the particle–wall gaps and depends on the prescribed wall velocity $\boldsymbol{g}$, but this dependence occurs only via the products $\boldsymbol{g}\cdot\boldsymbol{q}^i$, where $\boldsymbol{q}^i$ are perpendicular to the wall. Therefore, $\widehat{Q}$ would depend on the boundary conditions only if the prescribed velocity $\boldsymbol{g}$ has a component perpendicular to the wall. In the case of the shear boundary conditions, $\boldsymbol{g}$ is directed parallel to the walls, and thus all scalar products containing $\boldsymbol{g}$ in (3.2) vanish, and therefore it is easy to choose virtual trial velocities so that $\widehat{Q}$ is zero.

It is well known that solving the minimization problem for Q is equivalent to solving the linear algebraic system of equations (the so-called Euler–Lagrange equations), obtained by equating to zero all partial derivatives of Q in T^i_k, ω^i. The resulting linear system of equations (B 2), (B 7), presented in Appendix B, gives the force and torque balance for the particles, and the minimization of Q ensures that the rigid-body translational and angular velocities are chosen in such a way that the suspension is in mechanical equilibrium. The structure of the system (B 2), (B 7) can be seen by writing it in a compact form, as follows. Gathering the unknown components of the minimizing velocities $\boldsymbol{T}^i_{min}$ and ω^i_{min} in a single vector of unknowns $\boldsymbol{z}$, we can write the network equations as

$$\left(\delta^{-3/2}\boldsymbol{A} + \delta^{-1/2}\boldsymbol{B}\right)\boldsymbol{z} = \delta^{-3/2}\boldsymbol{f} + \delta^{-1/2}\boldsymbol{h}, \tag{3.6}$$

where $\boldsymbol{A}, \boldsymbol{B}$ are matrices that depend on $\boldsymbol{q}^{ij}$, $\boldsymbol{p}^{ij}$, and $\boldsymbol{q}^i$, $\boldsymbol{p}^i$, as well as on a and d_{ij}, d_i. Note that $\boldsymbol{A}, \boldsymbol{B}$ do not depend explicitly on δ, and their size remains bounded above as δ tends to zero. In fact, the size depends only on the number of particles N. We consider N as large but finite (smaller than the maximal close packing number).

The right-hand side of (3.6) corresponds to the terms of Q that depend on the given wall velocity $\boldsymbol{g}$, given by either (2.2) or (2.5), as well as on $\boldsymbol{q}^i$, $\boldsymbol{p}^i$, a and d_i. In particular, $\boldsymbol{f}$ depends on $\boldsymbol{g}$ only through the products $\boldsymbol{g}\cdot\boldsymbol{q}^i$, while $\boldsymbol{h}$ depends

on products $\boldsymbol{g}\cdot\boldsymbol{p}^i$. Therefore, as explained above, in the case of shear boundary conditions $\boldsymbol{f}=0$, which results in the weak blow-up of the effective shear viscosity $\mu^\star$. More details on the justification of the weak blow-up for $\mu^\star$ are given in § 3.2.

Let us now turn to a more complicated case of extensional conditions. In this case $\boldsymbol{f}\neq 0$ in (3.6), which means that the right-hand side of (3.6) contains terms of order $\delta^{-3/2}$. Therefore, in order to calculate the leading term in the asymptotics of λ^*, one could attempt to minimize the simpler functional $\widehat{Q}$. Similarly to (3.6), the minimizers $\widehat{\boldsymbol{T}}^i$ of the truncated functional $\widehat{Q}$ solve the following truncated system of equations

$$\boldsymbol{A}\boldsymbol{z}=\boldsymbol{f}, \tag{3.7}$$

A more explicit form of (3.7) (obtained from the minimization conditions $\partial\widehat{Q}/\partial T^i_k=0$) is

$$\sum_{j\in\mathcal{N}_i} C^{ij}_{sp}[(\widehat{\boldsymbol{T}}^i-\widehat{\boldsymbol{T}}^j)\cdot\boldsymbol{q}^{ij}]\boldsymbol{q}^{ij}+\boldsymbol{B}(\widehat{\boldsymbol{T}^i})=\boldsymbol{R}^i \quad (i=1,2,\ldots,N), \tag{3.8}$$

where

$$\boldsymbol{B}(\widehat{\boldsymbol{T}^i})=\begin{cases} C^i_{sp}(\widehat{\boldsymbol{T}^i}\cdot\boldsymbol{q}^i)\boldsymbol{q}^i & \text{when } i\in I,\\ 0 & \text{otherwise,}\end{cases} \tag{3.9}$$

and

$$\boldsymbol{R}^i=\begin{cases} C^i_{sp}(\boldsymbol{g}\cdot\boldsymbol{q}^i)\boldsymbol{q}^i & \text{when } i\in I,\\ 0 & \text{otherwise.}\end{cases} \tag{3.10}$$

The important computational issue related to (3.7) is that the matrix $\boldsymbol{A}$ is not invertible. Indeed, the homogeneous system corresponding to (3.8) has (infinitely many) non-trivial solutions. In particular, vectors of the form

$$\boldsymbol{T}^i=t\begin{pmatrix}1\\0\end{pmatrix} \tag{3.11}$$

solve this system for each real t.

From the computational point of view, the fact that the homogeneous system

$$\boldsymbol{A}\boldsymbol{z}=\boldsymbol{0} \tag{3.12}$$

has non-trivial solutions, implies by the standard results from linear algebra that determinant of $\boldsymbol{A}$ must be zero. Therefore, the non-homogeneous system (3.8) either has multiple solutions or else is non-solvable. It also follows from (3.11), (3.12) that any minimizer $\{\boldsymbol{T}^i\}, i=1,2,\ldots,N$ of $\widehat{Q}$ is not unique because it can be replaced by $\{\boldsymbol{T}^i+t(1,0)\}$ without changing the value of $\widehat{Q}$. It is very important to find out if the homogeneous system (3.12) has non-trivial solutions other than (3.11), since the presence of such solutions might signal that the algebraic procedure for evaluating the leading term will not in general produce a unique number. Therefore, it makes sense to look for conditions on the network which would guarantee that every solution of the homogeneous system is of the form (3.11). Then the non-homogeneous system (3.8) would be uniquely solvable up to horizontal translation. In § 3.3.2, we show that for a typical random distribution of particles this is indeed the case.

Then the above computational issue is resolved, the asymptotic order of the extensional viscosity depends on the validity of the estimate (3.5). The functional $\widehat{Q}$ is non-negative, but it may be zero. When (3.5) holds, local lubrication analysis provides the correct order of the leading term in the asymptotics of the extensional

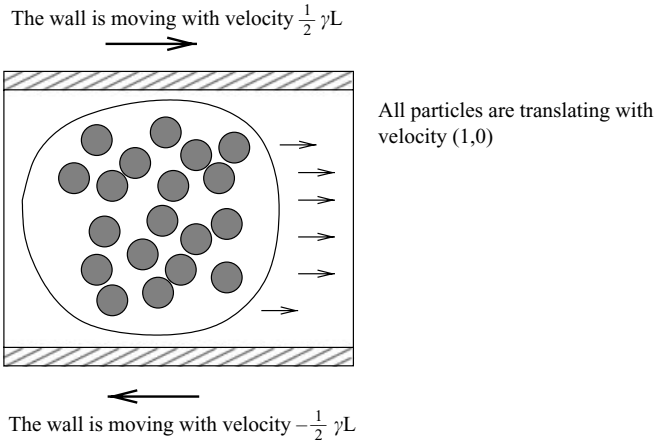

FIGURE 6. A cluster of particles moves as a rigid body in the horizontal direction. All the energy dissipation occurs in the boundary layers.

effective viscosity ($\delta^{-3/2}$ in dimension two and δ^{-1} in dimension three). If (3.5) does not hold, that is,

$$\min \widehat{Q} = 0, \tag{3.13}$$

then the leading term in the asymptotics of $\lambda^\star$ in dimension two is of order $\delta^{-1/2}$, ($\ln(1/\delta)$ in dimension three).

Whether or not the estimate (3.5) holds, depends on the geometry of the particle array as well as the boundary conditions on $\partial\Omega^+$ and $\partial\Omega^-$. In § 3.3.2, we show that in the case of extensional boundary conditions, (3.5) holds for generic arrays, and thus the leading term in the asymptotic of E_d (and extensional effective viscosity λ^*, see (2.18)) is of the order $\delta^{-3/2}$. However, for some special arrays, $\lambda^\star$ is of order $\delta^{-1/2}$. An example of such an array is presented in § 3.3.1.

The final remark concerns the physical meaning of velocities (3.11) in a shear flow. These velocities are compatible with the shear boundary conditions, for which the right-hand side in (3.7) is zero. This means that the shear boundary conditions do not contribute to the leading-order form $\widehat{Q}$, and can be viewed as zero boundary conditions on the scale $\delta^{-3/2}$. In this case, the velocities (3.11) correspond to a plane parallel flow of particles (so all the particles translate a single rigid body in the horizontal direction) while the walls of the apparatus move with different horizontal velocities. In that case, all the dissipation takes place in two thin boundary layers near the walls (see figure 6).

3.2. *Effective shear viscosity*

In this section we show that in dimension two, the asymptotic order of the shear effective viscosity $\mu^\star$ is $\delta^{-1/2}$, while the local lubrication analysis predicts the rate $\delta^{-3/2}$. Hereinafter, local analysis means using a lubrication approximation to approximate the dissipation rate in a single gap between two nearly touching neighbouring particles. In three dimensions, $\delta^{-1/2}$ and $\delta^{-3/2}$ should be replaced by, respectively, $\ln\delta^{-1}$ and δ^{-1} (see Berlyand *et al.* 2005*a*). The local analysis in three dimensions predicts (see Frankel & Acrivos 1967; Berlyand *et al.* 2005*a*) that the asymptotics of the shear effective viscosity $\mu^\star$ (see (2.15)) should be of order δ^{-1}, but numerical simulations of Sierou & Brady (2001) (their article also quotes experimental results of Van der Werff *et al.* 1989 and Shikata & Pearson 1994) show that random suspensions in shear flow

have effective viscosity of order $\ln \delta^{-1}$. Our estimate $\mu^\star = O(\delta^{-1/2})$ is therefore in agreement with the three-dimensional results in Sierou & Brady (2001), also showing the weak blow-up.

The decrease in the asymptotic order of $\mu^\star$ is a global phenomenon in the following sense. It shows that the local analysis could be misleading, and global analysis of the entire particle array is necessary.

In the case of the shear boundary conditions, the velocity at the boundary is oriented perpendicular to the particle–wall gaps, and thus $\boldsymbol{g}\cdot\boldsymbol{q}^i = 0$ for all such gaps. Consequently, the vectors $\boldsymbol{R}^i$ in (3.10) are zero, and the system (3.7) becomes homogeneous. This means that the shear boundary conditions do not produce strong blow-up of the dissipation rate, because the leading-order form $\widehat{Q}$ becomes $A\boldsymbol{z}\cdot\boldsymbol{z}$ which is clearly zero for every solution of the homogeneous system $A\boldsymbol{z} = 0$. We know that there are multiple non-trivial solutions of (3.12) given by (3.11). Moreover, the total dissipation rate E_d is given by a variational (minimization) principle for the full form Q. Therefore, to obtain an upper bound on E_d, it is sufficient to evaluate Q on any collection of admissible velocities compatible with the shear boundary conditions. In particular, we can take the trial velocities such that all $\boldsymbol{T}^i = 0$ and all $\omega^i = 0$. This collection makes $\widehat{Q}$ zero (since $\boldsymbol{T}^i = 0$ are of the general form (3.11)), and thus the leading term of Q degenerates. Substituting $\boldsymbol{T}^i = 0, \omega^i = 0$ into (2.26), (2.27) and summing up over all gaps, we obtain

$$\mu^\star = C E_d \leqslant C Q(\boldsymbol{T}^i = 0, \omega^i = 0) = C\delta^{-1/2} \sum_{i\in I} C^i_{sh} (\boldsymbol{g}\cdot\boldsymbol{p}^i)^2, \tag{3.14}$$

where $C = 2\gamma^{-2}|\Omega|^{-1}$ (see (2.15)), and the summation is over all particle–wall gaps. Next we note that $\boldsymbol{g}\cdot\boldsymbol{p}^i = \gamma$ for all values of i, which implies

$$\mu^\star \leqslant 2\delta^{-1/2}|\Omega|^{-1} \sum_{i\in I} C^i_{sh}. \tag{3.15}$$

Since the number of particle–wall gaps is finite, and the values of C^i_{sh} defined in (2.28) are independent of δ, we finally arrive at an upper bound on $\mu^\star$:

$$\mu^\star \leqslant C_1 \delta^{-1/2}, \tag{3.16}$$

where C_1 is independent of δ.

From the continuum mechanics point of view, zero velocity field corresponds to the flow in which all the particles form a motionless cluster, while the walls of the apparatus move with the horizontal velocities given by (2.2) (see figure 6, and set $t = 0$). Then the entire dissipation is produced in the two narrow boundary layers between the particle cluster and the walls, where the shear deformation takes place. Since classical lubrication approximation shows that the dissipation rate in such layers exhibits weak blow-up, the entire dissipation rate must exhibit weak blow-up. We emphasize that (3.15) is only an upper bound for μ^*, and by no means an approximation. The actual value of μ^* can be much smaller than the right-hand side of (3.15). Similarly, the zero-velocity particle field is not an approximation of the actual particle velocities that determine the exact value of μ^*. Calculation of actual velocities is a much more difficult task than estimating the minimum of Q from the above. The method of estimation provides us with a simple procedure for proving that the asymptotic order of μ^* cannot be larger than $\delta^{-1/2}$.

To understand better the nature of the actual flow, we find the exact velocity fields for a simple example of a two-disk network on figure 7, subject to the shear boundary

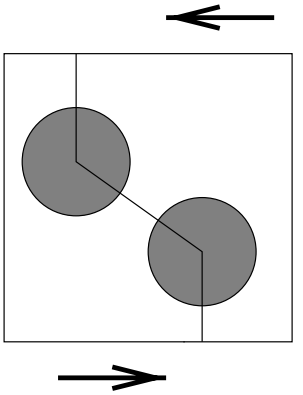

FIGURE 7. A two-disk network with shear boundary conditions.

conditions with $\gamma = 1$. The functional Q in this example can be written as follows

$$\begin{aligned} Q = {} & \delta^{-3/2}\{C^{12}_{sp}[(\boldsymbol{T}^1 - \boldsymbol{T}^2)\cdot \boldsymbol{q}^{12}]^2 + C^1_{sp}[(\boldsymbol{T}^1 - \boldsymbol{e}_1)\cdot \boldsymbol{e}_2]^2 + C^2_{sp}[(\boldsymbol{T}^2 + \boldsymbol{e}_1)\cdot \boldsymbol{e}_2]^2\} \\ & + \delta^{-1/2}\{C^{12}_{sh}[(\boldsymbol{T}^1 - \boldsymbol{T}^2)\cdot \boldsymbol{p}^{12} + a\omega_1 + a\omega_2]^2 + C^{12}_{rot}a^2(\omega_1 - \omega_2)^2\} \\ & + \delta^{-1/2}\{C^1_{sh}[(\boldsymbol{T}^1 - \boldsymbol{e}_1)\cdot \boldsymbol{e}_1 + a\omega_1]^2 + C^2_{sh}[(\boldsymbol{T}^2 + \boldsymbol{e}_1)\cdot \boldsymbol{e}_1 + a\omega_2]^2\} \\ & + \delta^{-1/2}\{4C^1_{rot}a^2{\omega_1}^2 + 4C^2_{rot}a^2{\omega_2}^2\}. \end{aligned} \tag{3.17}$$

For simplicity, we assume that D^1 and D^2 are located the same distance away from the boundary. In that case, $C^1_{sp} = C^2_{sp}$, $C^1_{sh} = C^2_{sh}$, $C^1_{rot} = C^2_{rot}$, so we can drop superscripts, and look for a solution such that $\boldsymbol{T}^2 = -\boldsymbol{T}^1 \equiv -\boldsymbol{T}$, $\omega^1 = \omega^2 \equiv \omega$. Next we write the minimization conditions $\partial Q/\partial T_k = 0$, $\partial Q/\partial \omega = 0$, and cancel the highest negative powers of δ. This yields the following network equations (compare with (3.6)):

$$\begin{aligned} & 2C^{12}_{sp}[\boldsymbol{T}\cdot \boldsymbol{q}^{12}]\boldsymbol{q}^{12} + C_{sp}[\boldsymbol{T}\cdot \boldsymbol{q}^1]\boldsymbol{q}^1 \\ & \qquad + \delta\{2C^{12}_{sh}[\boldsymbol{T}\cdot \boldsymbol{p}^{12} + a\omega]\,\boldsymbol{p}^{12} + C_{sh}[\boldsymbol{T}\cdot \boldsymbol{p}^1 + a\omega]\,\boldsymbol{p}^1\} = \delta C_{sh}\boldsymbol{e}_1, \end{aligned} \tag{3.18}$$

and

$$C^{12}_{sh}[\boldsymbol{T}\cdot \boldsymbol{p}^{12} + a\omega] + C_{sh}[\boldsymbol{T}\cdot \boldsymbol{p}^1 + a\omega] + 4aC_{rot}\omega = C_{sh}. \tag{3.19}$$

Next, we find $a\omega$ from (3.19) and substitute into (3.18). Then, projecting the vector equation (3.18) onto the coordinate axes produces two scalar equations for two components of $\boldsymbol{T}$:

$$\begin{aligned} & 2C^{12}_{sp}(\boldsymbol{T}\cdot \boldsymbol{q}^{12})q^{12}_1 + \delta[\boldsymbol{T}\cdot(\boldsymbol{p}^{12} - A^{-1}\boldsymbol{k})p^{12}_1 + \delta C_{sh}\boldsymbol{T}\cdot(\boldsymbol{p}^1 - A^{-1}\boldsymbol{k})] \\ & \qquad = \delta C_{sh}(1 - 2A^{-1}C_{sh}p^{12}_1 - A^{-1}C_{sh}), \end{aligned} \tag{3.20}$$

and

$$2C^{12}_{sp}(\boldsymbol{T}\cdot \boldsymbol{q}^{12})q^{12}_2 + C_{sp}\boldsymbol{T}\cdot \boldsymbol{e}_2 + \delta[\boldsymbol{T}\cdot(\boldsymbol{p}^{12} - A^{-1}\boldsymbol{k})p^{12}_2 + \delta C_{sh}\boldsymbol{T}\cdot(\boldsymbol{p}^1 - A^{-1}\boldsymbol{k})] = 0, \tag{3.21}$$

where $A = 2C^{12}_{sh} + C_{sh} + 4C_{rot}$, and $\boldsymbol{k} = 2C^{12}_{sh}\boldsymbol{p}^{12} + C_{sh}\boldsymbol{p}^1$. The system (3.20), (3.21) can be written concisely as

$$\boldsymbol{M}\boldsymbol{T} + \delta\boldsymbol{L}\boldsymbol{T} = \delta\boldsymbol{F}, \tag{3.22}$$

where the matrix

$$\boldsymbol{M} = 2C_{sp}^{12}\begin{pmatrix} \left(q_1^{12}\right)^2 & q_1^{12}q_2^{12} \\ q_1^{12}q_2^{12} & \left(q_2^{12}\right)^2 + C_{sp}\left(2C_{sp}^{12}\right)^{-1} \end{pmatrix} \tag{3.23}$$

has determinant $C_{sp}(q_1^{12})^2$, which is non-zero because $q_1^{12} \neq 0$ ($\boldsymbol{q}^{12}$ is non-vertical). Since $\boldsymbol{M}^{-1}$ exist, we can write

$$\boldsymbol{T} = \delta(\boldsymbol{I} + \delta\boldsymbol{M}^{-1}\boldsymbol{L})^{-1}\boldsymbol{M}^{-1}\boldsymbol{F} = \delta\sum_{j=0}^{\infty}\delta^j(\boldsymbol{M}^{-1}\boldsymbol{L})^j\boldsymbol{M}^{-1}\boldsymbol{F}, \tag{3.24}$$

which yields the following asymptotics.

$$\begin{aligned} \boldsymbol{T}^1 &= -\boldsymbol{T}^2 = \delta\boldsymbol{M}^{-1}\boldsymbol{F} + O(\delta^2) = O(\delta), \\ \omega^1 &= \omega^2 = \frac{C_{sh}}{aA} - \delta(aA)^{-1}\boldsymbol{M}^{-1}\boldsymbol{F}\cdot\boldsymbol{k} + O(\delta^2) = O(1), \end{aligned} \tag{3.25}$$

as $\delta \to 0$.

This example shows that small translational velocities (of order δ) may produce large dissipation (of order $\delta^{-1/2}$) as long as the velocities are oriented in the correct way, as in a local squeeze motion. By contrast, certain large velocities produce either no dissipation, or a dissipation of order one. Indeed, if both particles move as a single rigid body, then the dissipation due to this motion is zero, regardless of the velocity magnitude.

The objective of our paper is to find the overall dissipation rate rather than the local structure of the velocity field in particle shear flow. This example provides us with some insight, but not with the complete description of the local flow. Also, the particle velocities that appear in our discrete dissipation form are approximate: the smaller δ is, the better the approximation. The latter can be made precise since approximation of the dissipation rates (convergence in integral norms) implies an approximation of the corresponding velocity fields (point-wise convergence of a subsequence).

3.3. *Extensional effective viscosity*

3.3.1. *Simplification of boundary conditions*

In this section, we show that for the extensional boundary conditions, the leading term in the asymptotics of the dissipation rate E from (3.4) may or may not be zero, depending on the geometry of a particle array, that is, the leading term in the asymptotics of the effective extensional viscosity is either of order $\delta^{-3/2}$ (strong blow-up) or $\delta^{-1/2}$ (weak blow-up). We provide two geometric conditions on the network graph which ensure strong blow-up.

In a planar steady extensional flow of the effective fluid, the rate of strain tensor is

$$\boldsymbol{e}(\boldsymbol{v}^0) = \begin{pmatrix} \varepsilon & 0 \\ 0 & -\varepsilon \end{pmatrix}, \tag{3.26}$$

where ϵ denotes a constant extension rate. The corresponding velocity field is of the form

$$\boldsymbol{v}^0 = \begin{pmatrix} \varepsilon x_1 \\ -\varepsilon x_2 \end{pmatrix}, \tag{3.27}$$

which gives the boundary conditions

$$\boldsymbol{v}^0 = \begin{cases} \left(\varepsilon x_1, \frac{1}{2} - \varepsilon L\right) & \text{when } x_2 = L/2 = 1 \ \ (\text{on } \partial\Omega^+), \\ \left(\varepsilon x_1, \frac{1}{2}\varepsilon L\right) & \text{when } x_2 = -L/2 = -1 \ \ (\text{on } \partial\Omega^-). \end{cases} \tag{3.28}$$

We decompose $\boldsymbol{v}^0$ as

$$\boldsymbol{v}^0 = \boldsymbol{v}^0_{vc} + \boldsymbol{v}^0_{ge}, \tag{3.29}$$

where $\boldsymbol{v}^0_{vc}$ is a vertical contraction velocity satisfying

$$\boldsymbol{v}^0_{vc} = \boldsymbol{g}_{vc} = \begin{cases} -\varepsilon \boldsymbol{e}_2 & \text{on } \partial\Omega^+, \\ \varepsilon \boldsymbol{e}_2 & \text{on } \partial\Omega^-, \end{cases} \tag{3.30}$$

and $\boldsymbol{v}^0_{ge}$ is the horizontal extension velocity field with the boundary conditions given by

$$\boldsymbol{v}^0_{ge} = \boldsymbol{g}_{ge} = \begin{cases} \varepsilon x_1 \boldsymbol{e}_1 & \text{on } \partial\Omega^+, \\ \varepsilon x_1 \boldsymbol{e}_1 & \text{on } \partial\Omega^-. \end{cases} \tag{3.31}$$

Note that $\boldsymbol{g} = \boldsymbol{g}_{vc} + \boldsymbol{g}_{ge}$, and the boundary edges are orthogonal to the boundary ($\boldsymbol{g}_{ge} \perp \boldsymbol{q}^i, i \in I$). Therefore the value of $\widehat{Q}$ in (3.2) does not change when $\boldsymbol{g}$ in (3.2) is replaced by $\boldsymbol{g}_{vc}$, and we can write the total discrete dissipation form as

$$Q(\boldsymbol{T}^i, \omega^i, \boldsymbol{g}) = \delta^{-3/2}\widehat{Q}(\boldsymbol{T}^i, \boldsymbol{g}_{vc}) + \delta^{-1/2}Q'(\boldsymbol{T}^i, \omega^i, \boldsymbol{g}_{vc} + \boldsymbol{g}_{ge}), \tag{3.32}$$

where we have included an explicit dependence on the boundary conditions. To determine the rate of blow-up of the dissipation rate, we must analyse the minimizers of $\widehat{Q}(\boldsymbol{T}^i, \boldsymbol{g}_{vc})$. This form is rescaled in the sense that the leading-order term of Q is $\delta^{-3/2}\widehat{Q}$, and the coefficients of $\widehat{Q}$ do not depend on δ. This implies that the collection of velocities minimizing $\widehat{Q}$ is also independent of δ. Substitution of any such collection into the second term in the right-hand side of (3.32) yields a quantity of order $\delta^{-1/2}$ (at most). Since $\widehat{Q}$ is independent of δ, its minimizing vectors $\widehat{\boldsymbol{T}}^i$ are also δ-independent. Consequently, the blow-up rate of the dissipation depends on whether the minimum of $\widehat{Q}(\boldsymbol{T}^i, \boldsymbol{g}_{vc})$ is positive. If it is, the extensional effective viscosity $\lambda^\star$ is of order $\delta^{-3/2}$, otherwise $\lambda^\star$ grows no faster than $\delta^{-1/2}$. Which type of behaviour occurs, depends on the validity of the estimate (3.5). As mentioned in § 3.1, (3.5) may fail for certain particle arrays. In this section, we provide geometric conditions which ensure the positivity of $\min \widehat{Q}$, and give examples of networks for which this minimum is zero. The principal conclusion here is that extensional viscosity of suspensions with the same overall volume fraction of particles may vary by an order of magnitude in the interparticle distance, depending on the geometry of a particle array.

3.3.2. *Strong blow-up of $\lambda^\star$. Percolating rigidity networks*

For the rest of this section, we consider the steady flow of the suspension corresponding to the boundary conditions (3.30) with the extension rate $\varepsilon = 1$.

The network Γ partitions Ω into a disjoint union of polygons, called *Delaunay cells*. When points $\boldsymbol{x}^j$ are distributed randomly in Ω, the interior Delaunay cells are typically triangles. This simple but important fact can be explained as follows. The edges of Voronoi tessellation are perpendicular bisectors of the edges of Delaunay cells. If an interior Delaunay cell is, for instance, a quadrilateral, then any two vertices lying on a diagonal cannot be neighbours, and therefore the point of intersection of four edges of the Voronoi tessellation must be equidistant from the four vertices. This means that a convex quadrilateral may be a Delaunay cell only if all four vertices lie

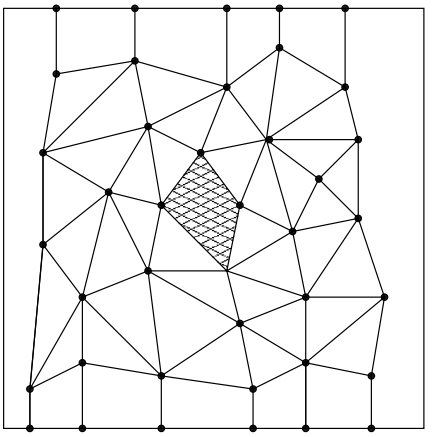

FIGURE 8. Delaunay cells of a generic network. The shaded quadrilateral represents a defect Delaunay cell.

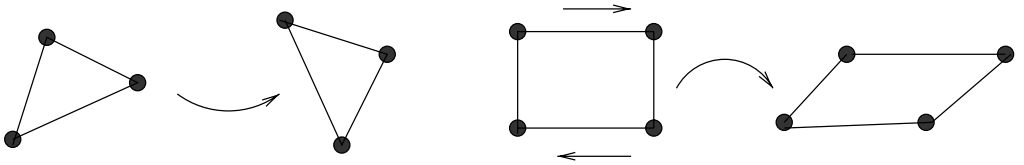

FIGURE 9. A triangle resists deformation, while a quadrilateral can be easily sheared without changing the side lengths.

on a circle. When the vertices of the network are randomly placed, the likelihood of four (or more) points lying on the same circle is small. It is natural to call such cells the defect cells. Therefore, most of the interior Delaunay cells of a random network are triangles. Other polygonal cells (quadrilateral, pentagonal etc.) are typically small in number, isolated and are likely to be unstable in the actual flow.

Since the boundary edges of the network are vertical, the cells adjacent to the boundary are typically quadrilateral. An example of a generic Delaunay network is shown in figure 8.

We now demonstrate that a typical geometric arrangement of small groups of three or four neighbouring particles can change the order of magnitude of the extensional effective viscosity. Specifically, consider two basic geometric structures in the network: a triangle and a quadrilateral in figure 9. When the lower-order terms in Q are neglected, we neglect the dissipation due to local rotations and shear, and take into account only the local squeeze flows. Therefore, a possible interpretation of the approximation $\delta^{-3/2}\widehat{Q} \approx Q$ is that local rotations of particles are dissipation-free. This leads us to picture the network as a framework of deformable bars, that are free to rotate around the joints (vertices of the network), while changing the lengths of the bars leads to strong dissipation. In this picture, the fundamental difference between a triangle and a quadrilateral becomes clear. A triangle cannot be deformed without changing the lengths of the sides. In contrast, a quadrilateral easily changes its shape under shear without changing the lengths of the sides and thus without an increase in the approximate dissipation rate. We can say that a triangle is rigid, whereas a quadrilateral is flexible. The three simple examples that make these notions rigorous are provided in Appendix C.

Clusters of connected triangles support the squeeze mode in the sense that the corresponding bar framework cannot be easily compressed, so extensional (or compressional) deformation of the corresponding particle array leads to strong dissipation of order $\delta^{-3/2}$. If a network contains enough interconnected triangular cells to span the whole network, then such a network is called *quasi-triangulated*. Because of the structural properties of Delaunay-type networks, a generic network is quasi-triangulated. For such networks, the leading term in the asymptotics $\lambda^\star$ can be effectively computed by minimizing the form $\widehat{Q}$, that is, the minimum is unique and can be found by solving the truncated linear system (3.7), and the solution obtained is unique up to a uniform horizontal translation.

Our results concerning the estimate (3.5) apply to an even broader class of networks called *percolating rigidity networks*. In these networks, the number of triangular cells may be relatively small, as indicated by the examples below. Percolating rigidity is ensured by the presence of a spanning quasi-triangulated subgraph which we call a *rigid backbone*. In a typical Delaunay network, the defect cells are likely to be isolated, so that the backbone coincides with the whole graph. However, a much smaller backbone is sufficient to ensure percolating rigidity. In particular, a backbone might have the form of a triangulated path in figure 11. Using techniques from linear algebra, we can show that the extensional effective viscosity $\lambda^\star$ of suspensions corresponding to such networks is $O(\delta^{-3/2})$. The necessary definitions and proofs are presented in Appendix D. The main idea of the proofs is based on the following observation. The dissipation form $\widehat{Q}(\boldsymbol{T}^i, \boldsymbol{g}_{vc})$ is a sum of non-negative terms, namely

$$\widehat{Q}(\boldsymbol{T}^i, \boldsymbol{g}_{vc}) = \frac{1}{2}\sum_{i=1}^{N}\sum_{j\in\mathcal{N}_i} C_{sp}^{ij}((\boldsymbol{T}^i - \boldsymbol{T}^j)\cdot\boldsymbol{q}^{ij})^2 + \sum_{i\in I} C_{sp}^{i}((\boldsymbol{T}^i - \boldsymbol{g}_{vc})\cdot\boldsymbol{q}^{i})^2. \tag{3.33}$$

This shows that $\min \widehat{Q}(\boldsymbol{T}^i, \boldsymbol{g}_{vc}) = 0$ if and only if all the quadratic terms in (3.33) are zero, or, equivalently, the minimizing vectors $\boldsymbol{T}^i, i = 1, 2, \ldots, N$ satisfy the system of equations

$$(\boldsymbol{T}^i - \boldsymbol{T}^j)\cdot\boldsymbol{q}^{ij} = 0 \quad (i = 1, 2, \ldots, N,\ j \in \mathcal{N}_i), \tag{3.34a}$$

$$(\boldsymbol{T}^i - \boldsymbol{g}_{vc})\cdot\boldsymbol{q}^{i} = 0 \quad (i \in I). \tag{3.34b}$$

Hence, if (3.34) does not have solutions, (3.5) must hold. It is important to point out that (3.34) is much simpler than the network equations. Its physical meaning is as follows. If a collection of $\boldsymbol{T}^i$ solves (3.34) then the relative velocities $\boldsymbol{T}^i - \boldsymbol{T}^j$ are oriented perpendicular to $\boldsymbol{q}^{ij} = (\boldsymbol{x}^i - \boldsymbol{x}^j)/|\boldsymbol{x}^i - \boldsymbol{x}^j|$. Therefore, solutions of (3.34) correspond to local shear motions. Therefore, the leading term of the discrete dissipation form degenerates exactly when applying extensional boundary conditions induces local shear motions of all pairs of neighbouring particles.

Also, it should be noted that if the estimate (3.5) holds for some subnetwork, then it also holds for the whole network. This is clearly seen from (3.33), because a subnetwork is obtained from the full network by removing some edges. Since each edge corresponds to a non-negative term in the dissipation form, we can decrease dissipation only by removing edges. This observation can be used to reduce the network to a simpler subnetwork for which it is easier to determine whether (3.5) holds.

Examples of quasi-triangulated and percolated rigidity graphs are presented in figures 10 and 11. First, we observe that a restriction to Ω of a periodic rectangular

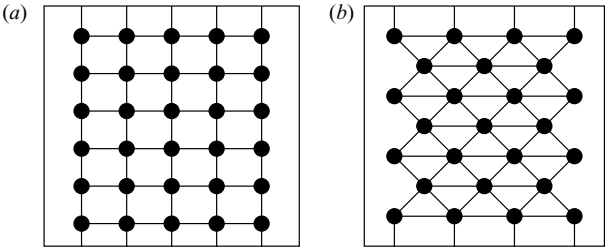

FIGURE 10. (*a*) A rectangular graph is not quasi-triangulated. (*b*) A triangular graph is quasi-triangulated.

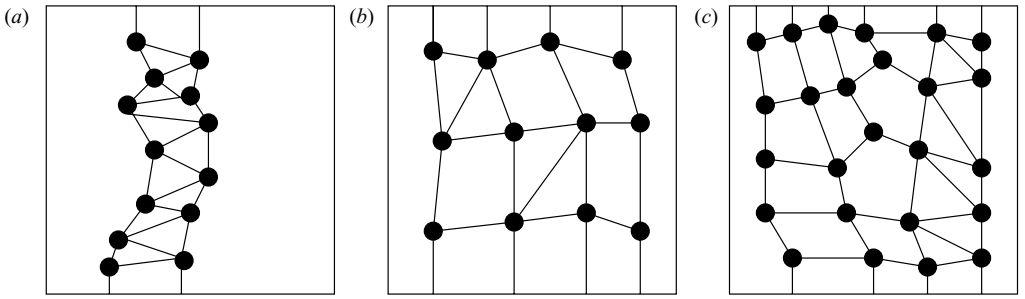

FIGURE 11. (*a*) A triangulated path. This percolating rigidity network is quasi-triangulated. (*b*) A percolating rigidity network that does not contain a triangulated path. (*c*) A network that contains a triangulated path (and thus possesses percolating rigidity), but is not quasi-triangulated.

lattice is not quasi-triangulated. By contrast, a periodic triangular lattice restricted to Ω is quasi-triangulated (see figure 10).

Generally, if a network is not periodic, but all of its interior Delaunay cells are triangles, then this network is quasi-triangulated. However, a quasi-triangulated network is not necessarily a triangulation, because some defect cells may still occur. An example in figure 11 shows that the fraction of the defect cells may be rather large.

We now present another class of percolating rigidity networks: networks that contain a path connecting $\partial\Omega^+$ and $\partial\Omega^-$, such that all edges in this path are oriented along the $\boldsymbol{e}_2$-direction (vertical). A simple example is a periodic square lattice oriented parallel to the sides of Ω (figure 10*a*). This network does not have a triangulated rigid backbone, but the leading term of the discrete dissipation form is still non-degenerate. To explain this, we can use the above mentioned analogy with a bar framework. Clearly, applying the extensional boundary conditions to a vertical path of bars makes them compress and thus produces strong blow-up. Consequently, the asymptotics of the extensional effective viscosity is of order $\delta^{-3/2}$ (strong blow-up of $\lambda^\star$. Asymptotic formulae of Nunan & Keller (1984) also predict strong blow-up of the extensional viscosity for cubic lattices. Thus, our results are consistent with the results of Nunan & Keller. See § 3.4 for a more detailed comparison, and Appendix E for a more general criterion of this type and the proof of strong blow-up.

The above considerations show that the strong blow-up of $\lambda^\star$ is generic. However, it is possible to construct special particle arrays for which the leading term in the asymptotics of $\lambda^\star$ is zero. A simple example of such an array is a rectangular lattice rotated so that none of its interior edges is vertical. Let $\boldsymbol{k}$ denote a unit vector that is parallel to neither $\boldsymbol{e}_1$ nor $\boldsymbol{e}_2$. The interior edges of the rectangular network in

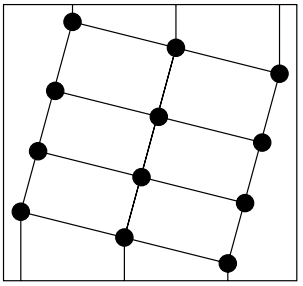

FIGURE 12. A rotated rectangular lattice of 12 vertices.

figure 12 are either parallel or perpendicular to $\boldsymbol{k}$, while the prescribed boundary velocities are parallel to $\boldsymbol{e}_2$. This misalignment will lead to weak blow-up. Here we follow the general strategy outlined in § 3.3.2. To show that $\min \widehat{Q} = 0$, it is enough to find non-trivial velocities $\boldsymbol{T}^i$ that solve the system (3.34). This is done in Appendix E.

3.4. *Comparison with some results for periodic cubic arrays in dimension three*

The main objective of the network approximation is to define effective properties for non-periodic deterministic or random arrays. Although techniques of periodic homogenization are well developed (Bensoussan, Lions & Papanicolaou 1978; Sanchez-Palencia 1980; Jikov, Kozlov & Oleinik 1994 and references therein), non-periodic geometries are much less understood. At the end of this section, we compare our results applied in the particular case of a periodic square array (in dimension two) with the results of Nunan & Keller (1984) for cubic arrays in dimension three.

The effective viscosity of an infinite periodic suspension obtained by Nunan & Keller (1984) is the fourth-order tensor $\boldsymbol{\mu}^\star$ (in this section, we use the notation from Nunan & Keller 1984). In an effective flow with the constant strain rate γ, the effective stress is

$$S^0_{ij} = 2\mu^\star_{ijkl}\gamma_{kl} - P\delta_{ij}, \tag{3.35}$$

where P is an effective pressure. Hereinafter, summation over repeated indices is assumed. Nunan & Keller (1984) obtained the following formula for the components of $\boldsymbol{\mu}^\star$:

$$\mu^\star_{ijkl} = \tfrac{1}{2}\mu(1+\beta)\big(\delta_{ik}\delta_{jl} + \delta_{il}\delta_{jk} - \tfrac{2}{3}\delta_{ij}\delta_{kl}\big) + \mu(\alpha-\beta)\big(\delta_{ijkl} - \tfrac{1}{2}\delta_{ij}\delta_{kl}\big), \tag{3.36}$$

where δ_{ij} is equal to one if $i = j$, and zero otherwise. Also, $\delta_{ijkl} = 1$ if all indices are equal, otherwise $\delta_{ijkl} = 0$. The term μ is the fluid viscosity, and α, β are functions of the small parameter ϵ, related to the typcial interparticle distance δ as follows:

$$\epsilon = \frac{\delta}{2a+\delta} \approx \frac{\delta}{2a} \quad \text{as } \delta \to 0. \tag{3.37}$$

(Note that this is true for periodic arrays, and may not hold for the more general arrays considered in the paper.) When the effective flow is incompressible, $\gamma_{ii} = 0$, so (3.36) simplifies to

$$\mu^\star_{ijkl} = \tfrac{1}{2}\mu(1+\beta)(\delta_{ik}\delta_{jl} + \delta_{il}\delta_{jk}) + \mu(\alpha-\beta)\delta_{ijkl}. \tag{3.38}$$

For simple cubic lattices, up to the terms of order $O(1)$ in ϵ (Nunan & Keller 1984),

$$\alpha = \tfrac{3}{16}\pi\epsilon^{-1} + \tfrac{27}{80}\pi\ln\epsilon^{-1}, \tag{3.39}$$

and

$$\beta = \tfrac{1}{4}\pi\ln\epsilon^{-1}. \tag{3.40}$$

Suppose that the imposed effective flow is a steady shear with the velocity $\boldsymbol{v} = (\kappa x_3, 0, 0)$ (three-dimensional analogue of (2.3)), where $\kappa > 0$ is a constant shear rate. The components of the corresponding strain rate tensor $\boldsymbol{\gamma}$ are $\gamma_{13} = \gamma_{31} = \kappa > 0$ and $\gamma_{ij} = 0$ for other values of (i, j). Then, using (3.38), we obtain from (3.35) that the only non-zero components of the effective deviatoric stress tensor $2\boldsymbol{\mu}^\star\boldsymbol{\gamma}$ are

$$(2\mu^\star\gamma)_{13} = (2\mu^\star\gamma)_{31} = 2\mu(1+\beta)\kappa. \tag{3.41}$$

Since α is not present in (3.41), the non-zero components of the deviatoric effective stress are of order $\ln\epsilon^{-1}$, and thus the shear effective viscosity calculated by the three-dimensional analogue of definition (2.15) is of order $\ln\epsilon^{-1}$ (weak blow-up in dimension three). The weak blow-up was not identified in Nunan & Keller (1984), but it can easily be deduced from the formulae derived there.

In the case of an extensional flow, velocity vector $\boldsymbol{v} = (\kappa x_1, \kappa x_2, -2\kappa x_3)$, (compare with (2.4)), where $\kappa > 0$ is a constant extension rate. The strain rate tensor is

$$\boldsymbol{\gamma} = \begin{pmatrix} \kappa & 0 & 0 \\ 0 & \kappa & 0 \\ 0 & 0 & -2\kappa \end{pmatrix}. \tag{3.42}$$

Then, using (3.35) and (3.38) we obtain the deviatoric stress

$$2\boldsymbol{\mu}^\star\boldsymbol{\gamma} = \begin{pmatrix} L & 0 & 0 \\ 0 & L & 0 \\ 0 & 0 & -2L, \end{pmatrix}, \tag{3.43}$$

where

$$L = 2\kappa\mu(1+\beta) + \kappa\mu(\alpha-\beta). \tag{3.44}$$

Components of the deviatoric stress contain α and are therefore of order ϵ^{-1}. Consequently, the extensional effective viscosity is of order ϵ^{-1} (strong blow-up in dimension three).

Although Nunan & Keller (1984) did not address the issue of weak versus strong blow-up for the effective viscosity, (3.39)–(3.44) are consistent with the results for square lattices in § 3.3.2 of this paper in the following sense. If a periodicity cell corresponding to a simple cubic lattice is subjected to a uniform shear (extensional) flow, then the straightforward calculation presented above shows that the shear (extensional) effective viscosity exhibits weak (strong) blow-up. However, for other lattice types such as body centred cubic (BCC) and face centred cubic (FCC), formulae from Nunan & Keller (1984) imply strong blow-up of both viscosities, whereas our approach leads to the weak blow-up of the shear viscosity for all two-dimensional lattices. There are two reasons for this. (i) In Nunan & Keller (1984), effective viscosity is defined for unbounded periodic arrays. Our definition is different because it takes into account boundary effects which are known to be essential in rheological measurements. (ii) In Nunan & Keller (1984), the particle velocities are specified beforehand (see their formulae (5) and (6)). These formulae imply that translational velocities of the particles are exactly the imposed shear flow velocities, and angular velocity is the same for all particles. It is not clear if such particle velocities occur in actual flows. In BCC and FCC lattices, this choice of particle velocities gives rise to local squeezing flows, and thus to strong blow-up.

We conclude this section with a brief summary of relevance of two-dimensional calculations for three-dimensional suspensions, and their limits of validity. First, we

observe that the issue of weak versus strong blow-up is qualitatively the same in both two and three dimensions. The only difference is quantitative: while strong and weak blow-up in three dimensions has singularities δ^{-1} and $\ln(\delta^{-1})$, respectively, the analogous singularities in two dimensions are $\delta^{-3/2}$ and $\delta^{-1/2}$.

There is one essential difference. In two dimensions, for typical arrays of disks, the gaps separate the fluid domain into a large number of disconnected (isolated) triangular regions, which may have different pressures. This creates local pressure gradients across the gaps (in the direction $\boldsymbol{p}^{ij}$, see figure 3) and may cause Poiseuille-like flow (seepage) of fluid across the gaps. The effect of Poiseuille-like flows in two dimensions has been investigated by Berlyand, Gorb & Novikov (2005*b*). By contrast, in three dimensions, the flow region outside the gaps is connected, and the analogous local pressure gradients do not arise.

This justifies the use of two-dimensional analysis (which is technically simpler) in the three-dimensional suspension problem.

4. Conclusions

We have studied finite size and particle–wall effects in effective rheology of concentrated non-colloidal suspensions with complex geometry. A small interparticle distance parameter δ was used to describe the high-concentration regime for particle arrays which are not necessarily periodic (i.e. random).

Our approach is to approximate the dissipation rate of a continuum system by its discrete analogue, the discrete dissipation form. This approximation was developed, and the leading term was rigorously justified, by Berlyand *et al.* (2005*a*). We use the discrete approximation for the dissipation rate to obtain the approximations of the shear ($\mu^\star$) and extensional ($\lambda^\star$) effective viscosities. Analysis of asymptotic behaviour (weak *vs.* strong blow-up) is the main subject of this paper. We have demonstrated that the discrete approximation is efficient in this analysis. The focus of the investigation is on suspensions of finite size, where the effective viscosity is strongly influenced by the particle–wall effects, or equivalently, by the prescribed conditions on the external boundary of the flow. Accordingly, the presence of two viscosities, even for a random macroscopically isotropic array, can be attributed to the cubic anisotropy due to two types of external boundary condition (shear and squeeze) applied in two perpendicular directions. This phenomenon would not be present in an infinite macroscopically isotropic array where the effective viscosity would be represented by a single scalar quantity. The difference between the finite- and infinite-size cases supports the view of Sierou & Brady (2002) that the notion of a 'universal' effective viscosity curve is questionable. Indeed, the measurable effective properties are not purely material constants, but may incorporate the effects due to the finite size of the apparatus.

Sierou & Brady (2001) calculated the high-frequency dynamic viscosity of concentrated suspensions as a function of volume fraction ϕ by means of accelerated Stokesian dynamics simulations. Numerical results indicate a singular behaviour of the effective viscosity as ϕ approaches the maximal close-packing fraction ϕ_{rcp}. We quote here from (Sierou & Brady (2001): 'The exact form of this singular behaviour is not known. Results from lubrication theory for cubic lattices would suggest that the singular form should consist both of $1/\epsilon$ and $\ln\epsilon^{-1}$, where $\epsilon = 1 - (\phi/\phi_{rcp})^{1/3}$, but the relative amount of each term is unknown... As far as we are able to tell at this point, the $\ln\epsilon^{-1}$ behaviour accurately describes the numerical data.'

One our objectives was to address the issue of the unexpectedly weak blow-up in Sierou & Brady (2001), and determine the asymptotic order of the effective viscosity coefficients as $\delta \to 0$. Our analysis of the shear viscosity $\mu^\star$, based on the discrete network approximation, showed that $\mu^\star = O(\delta^{-1/2})$ as $\delta \to 0$, while the local lubrication analysis in a single gap between two particles gives a higher rate $O(\delta^{-3/2})$. In dimension three, the corresponding rates, given by the network approximation, are, respectively, $\ln \delta^{-1}$ and δ^{-1} (see Berlyand *et al.* 2005*a*). Thus, our analysis offers a theoretical explanation of the weak blow-up of the shear viscosity. We also present a simple example of the flow that exhibits weak blow-up of $\mu^\star$. This example suggests that in the actual suspension shear flow, the particles rotate with finite angular velocities while their translational velocities scale as δ.

The asymptotic order of the extensional viscosity $\lambda^\star$ depends on the geometry of the particle array. For generic disordered arrays, the network partitions the domain into polygons (Delaunay cells), most of which are triangles. We have showed that for these generic arrays $\lambda^\star = O(\delta^{-3/2})$. The same asymptotic rate is obtained for a larger class of networks called quasi-triangulated. In a quasi-triangulated network, the percentage of triangular cells may be relatively small, but the subnetwork containing triangular cells must be spanning. Another class of networks for which $\lambda^\star = O(\delta^{-3/2})$, consists of rectangular periodic arrays aligned with the boundary of the flow. More generally, the same rate is obtained for arrays containing a single spanning chain of neighbouring particles, perpendicular to the part of the boundary where the velocity is prescribed.

We show that for strong blow-up, the leading term in the asymptotics of $\lambda^\star$ can be uniquely determined by solving a simplified linear system of the network equations, provided that the array is quasi-triangulated. Such a simplified system provides an efficient computational tool for evaluating the dependence of the effective viscosity on the geometry of the particle array and external boundary conditions. We also present an example of a network which exhibits weak blow-up of $\lambda^\star$.

Our results imply that the ratio of $\lambda^\star$ to $\mu^\star$ for generic disordered particle arrays is $O(\delta^{-1})$. Since $\mu^\star$ is proportional to an off-diagonal component of the effective stress, and $\lambda^\star$ is proportional to the effective normal stress difference, our results indicate non-Newtonian behaviour of the effective fluid. This conclusion agrees with the results of Sierou & Brady (2002) who detected a non-Newtonian effective rheology by numerically calculating normal stress differences under shear boundary conditions.

The authors wish to thank Professor John F. Brady for bringing the work of Sierou & Brady (2001) to their attention. L. B. was supported in part by NSF grant DMS-0204637. A. P. was supported in part by ONR grant N00014-001-0853 and by DOE grant DE-FG02-05ER25709.

Appendix A. Shear and extensional flows. Ratio of the viscosities in a Newtonian fluid

The following types of flow are relevant to our investigation.

Shear flow. Consider the steady shear flow of a homogeneous fluid characterized by the constant shear rate γ. The velocity is given by (2.3) and the strain rate tensor is

$$\mathbf{e}^0_{sh} = \frac{1}{2}\begin{pmatrix} 0 & \gamma \\ \gamma & 0 \end{pmatrix}. \tag{A 1}$$

Since the stress tensor is symmetric and independent of $\boldsymbol{x}$,

$$E^0 = \int_\Omega \boldsymbol{S}^0 \cdot \boldsymbol{e}^0_{sh}\, \mathrm{d}\boldsymbol{x} = \tfrac{1}{2} S^0_{12} \gamma |\Omega|, \tag{A 2}$$

where $|\Omega| = \int_\Omega \mathrm{d}\boldsymbol{x}$.

In the case of a homogeneous Newtonian fluid with viscosity μ, $\boldsymbol{S}^0 = 2\mu \boldsymbol{e}^0_{sh} - P\boldsymbol{I}$, so that $S^0_{12} = \mu\gamma$. Using (2.14), we obtain

$$\mu^\star = \mu, \tag{A 3}$$

as expected.

Extensional flow. In this case, the fluid is being extended in the horizontal direction and simultaneously contracted in the vertical direction at the same constant rate ε. The velocity is given by (2.4) and the strain rate is

$$\boldsymbol{e}^0_{ext} = \begin{pmatrix} \varepsilon & 0 \\ 0 & -\varepsilon \end{pmatrix}. \tag{A 4}$$

For a homogeneous Newtonian fluid, $\boldsymbol{S}^0_{ext} = 2\mu \boldsymbol{e}^0_{ext} - P\boldsymbol{I}$, and thus $S^0_{11} = 2\mu\varepsilon - P$, $S^0_{22} = -2\mu\varepsilon - P$. Next, using (2.17), we obtain

$$\lambda^\star = 4\mu. \tag{A 5}$$

Therefore, for a Newtonian effective fluid the ratio $\lambda^\star/\mu^\star$ is equal to 4 (in two dimensions).

Appendix B. Full system of the network equations

The sum of the local dissipation forms W^{ij}, W^i in (2.26), (2.27) gives the global (discrete) dissipation form

$$\begin{aligned} Q &= \sum_{\Pi_{ij}} W^{ij} + \sum_{\Pi_i} W^i \\ &= \sum_{i=1}^{N} \sum_{\substack{j \in \mathcal{N}_i \\ j<i}} \{\delta^{-3/2} C^{ij}_{sp} [(\boldsymbol{T}^i - \boldsymbol{T}^j)\cdot \mathbf{q}^{ij}]^2 + \delta^{-1/2} C^{ij}_{sh} [(\boldsymbol{T}^i - \boldsymbol{T}^j)\cdot \boldsymbol{p}^{ij} + a\omega^i + a\omega^j]^2 \\ &\quad + \delta^{-1/2} C^{ij}_{rot} a^2 (\omega^i - \omega^j)^2\} + \sum_{i\in I} \{\delta^{-3/2} C^i_{sp} [(\boldsymbol{T}^i - \mathbf{g})\cdot \boldsymbol{q}^i]^2 + \delta^{-1/2} C^i_{rot} a^2 (2\omega^i)^2 \\ &\quad + \delta^{-1/2} C^i_{sh} [(\boldsymbol{T}^i - \boldsymbol{g})\cdot \boldsymbol{p}^i + a\omega^i]^2\}, \end{aligned} \tag{B 1}$$

where I denotes the set of indices of the vertices adjacent to the boundary.

Although (B 1) accounts for three elementary motions depicted in figure 5, it does not account for a local motion when fluid moves between two motionless disks. This corresponds to the Poiseuille-type flow in a narrow channel whose upper and lower walls are curved. Since we focus on modelling viscometric experiments using boundary conditions (2.2), (2.5) (with no macroscopic pressure gradient imposed), contribution of these flows is not significant for three-dimensional suspensions. As explained in § 1, our goal here is study three-dimensional suspensions using a two-dimensional model for technical simplicity.

Note that in a physically two-dimensional problem (uniaxial rigid rods in a fluid) this contribution may no longer be negligible, as shown in Berlyand *et al.* (2005*b*). Indeed, in two dimensions, for typical arrays of disks (see figure 8), the gaps separate

the fluid domain into a large number of disconnected (isolated) triangular regions, which may have different pressures. This creates local pressure gradients across the gaps (in the direction $\boldsymbol{p}^{ij}$, see figure 3) and leads to a Poiseuille-like flow (seepage) of fluid across the gaps. By contrast, in three dimensions, the flow region outside the gaps is connected, and the analogous local pressure gradients do not arise.

It is well known that solving the minimization problem for Q is equivalent to solving the linear system (Euler–Lagrange equations), which is obtained by equating the gradient of Q to zero. Setting partial derivatives to zero with respect to T_l^i, $l = 1, 2$ we obtain

$$\sum_{j\in\mathcal{N}_i} \{\delta^{-3/2} C_{sp}^{ij}[(\boldsymbol{T}^i - \boldsymbol{T}^j)\cdot\boldsymbol{q}^{ij}]\boldsymbol{q}^{ij}\} + \sum_{j\in\mathcal{N}_i} \{\delta^{-1/2} C_{sh}^{ij}[(\boldsymbol{T}^i - \boldsymbol{T}^j)\cdot\boldsymbol{p}^{ij} + a\omega^i + a\omega^j]\boldsymbol{p}^{ij}\} + \boldsymbol{B}^i = \boldsymbol{F}^i, \tag{B 2}$$

for each $i = 1, 2, \ldots, N$, where

$$\boldsymbol{B}^i = \begin{cases} \delta^{-3/2} C_{sp}^i(\boldsymbol{T}^i\cdot\boldsymbol{q}^i)\boldsymbol{q}^i + \delta^{-1/2} C_{sh}^i[\boldsymbol{T}^i\cdot\boldsymbol{p}^i + a\omega^i]\boldsymbol{p}^i & \text{if } i\in I, \\ \boldsymbol{0} \quad \text{otherwise,} \end{cases} \tag{B 3}$$

(B 4)

$$\boldsymbol{F}^i = \begin{cases} \delta^{-3/2} C_{sp}^i(\boldsymbol{g}\cdot\boldsymbol{q}^i)\boldsymbol{q}^i + \delta^{-1/2} C_{sh}^i(\boldsymbol{g}\cdot\boldsymbol{p}^i)\boldsymbol{p}^i & \text{if } i\in I, \\ \boldsymbol{0} \quad \text{otherwise.} \end{cases} \tag{B 5}$$

(B 6)

Next, equating the partial derivatives $\partial Q/\partial\omega^i$ to zero, we obtain

$$\sum_{j\in\mathcal{N}_i} \{\delta^{-1/2} C_{sh}^{ij}[(\boldsymbol{T}^i - \boldsymbol{T}^j)\cdot\boldsymbol{p}^{ij} + a\omega^i + a\omega^j]\} + \sum_{j\in\mathcal{N}_i} \{\delta^{-1/2} C_{rot}^{ij}(\omega^i - \omega^j)\} + \mathscr{B}^i = \mathscr{M}^i, \tag{B 7}$$

for all $i = 1, \ldots, N$, where

$$\mathscr{B}^i = \begin{cases} \delta^{-1/2} C_{sh}^i(\boldsymbol{T}^i\cdot\boldsymbol{p}^i + a\omega^i) + 4\delta^{-1/2} C_{rot}^i\omega^i & \text{if } i\in I, \\ 0 \quad \text{otherwise.} \end{cases} \tag{B 8}$$

$$\mathscr{M}^i = \begin{cases} \delta^{-1/2} C_{sh}^i(\boldsymbol{g}\cdot\boldsymbol{p}^i) & \text{if } i\in I, \\ 0 \quad \text{otherwise.} \end{cases} \tag{B 9}$$

Equations (B 2) and (B 7) are, respectively, the equations of force and torque balance of the particles, and the minimization in (B 1) ensures that the rigid-body translational and angular velocities are chosen in such a way that the suspension is in mechanical equilibrium. Note also that (B 2) is a system of $2N$ equations, and (B 7) is a system of N equations. Together they form $3N$ equations for $3N$ unknowns $(\boldsymbol{T}^i, \omega^i)$. The coefficients and right-hand side of (B 2) are of order $\delta^{-3/2}$ and $\delta^{-1/2}$ whereas all the coefficients in (B 7) are of order $\delta^{-1/2}$. When all $\boldsymbol{T}^i$ are zero (no translations), the remaining terms are of order $\delta^{-1/2}$, but in the case $\omega^i = 0, i = 1, 2, \ldots, N$ (no rotations), the remaining equations contain terms of order $\delta^{-3/2}$. This reflects the well-known fact that the contributions from local translational spring motions are stronger than the contributions from rotational and other translational motions.

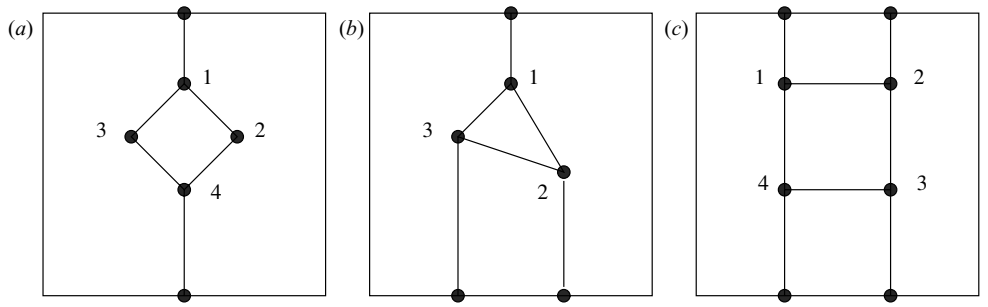

FIGURE 13. Three simple networks. (*a*) $\widehat{E} = 0$. (*b*, *c*) $\widehat{E} > 0$.

Appendix C. Simple examples of rigidity and flexibility

Suppose that the boundary conditions are given by (3.30) with $\varepsilon = -1$. In this section, we present three simple examples of networks with small numbers of vertices. One of these networks has $\widehat{E} = 0$, and the other two examples have $\widehat{E} > 0$.

Example 1. Consider the network in figure 13(*a*). This an example of a network for which $\widehat{E} = 0$. To demonstrate this, we show that there is a non-trivial particle velocity vector z such that $\widehat{Q}(z) = 0$.

The vectors $\boldsymbol{q}^{ij}$ are defined as follows.

$$\left.\begin{array}{c} \boldsymbol{q}^1 = \boldsymbol{e}_2, \boldsymbol{q}^4 = -\boldsymbol{e}_2, \\ \boldsymbol{q}^{12} = \boldsymbol{q}^{34} = \frac{1}{\sqrt{2}}(\boldsymbol{e}_1 - \boldsymbol{e}_2), \\ \boldsymbol{q}^{13} = \boldsymbol{q}^{24} = -\frac{1}{\sqrt{2}}(\boldsymbol{e}_1 + \boldsymbol{e}_2) \end{array}\right\} \tag{C 1}$$

Next, define $\boldsymbol{T}^i$ as follows.

$$\boldsymbol{T}^1 = \boldsymbol{e}_2, \quad \boldsymbol{T}^2 = -\boldsymbol{e}_1, \quad \boldsymbol{T}^3 = \boldsymbol{e}_1, \quad \boldsymbol{T}^4 = -\boldsymbol{e}_2. \tag{C 2}$$

The functional $\widehat{Q}$ corresponding to this network is

$$\begin{aligned} \widehat{Q} = {} & C^1_{sp}[(\boldsymbol{T}^1 - \boldsymbol{e}_2)\cdot\boldsymbol{q}^1]^2 + C^{12}_{sp}[(\boldsymbol{T}^1 - \boldsymbol{T}^2)\cdot\boldsymbol{q}^{12}]^2 \\ & + C^{13}_{sp}[(\boldsymbol{T}^1 - \boldsymbol{T}^3)\cdot\boldsymbol{q}^{13}]^2 + C^{24}_{sp}[(\boldsymbol{T}^2 - \boldsymbol{T}^4)\cdot\boldsymbol{q}^{24}]^2 \\ & + C^{34}_{sp}[(\boldsymbol{T}^3 - \boldsymbol{T}^4)\cdot\boldsymbol{q}^{34}]^2 + C^4_{sp}[(\boldsymbol{T}^4 + \boldsymbol{e}_2)\cdot\boldsymbol{q}^4]^2. \end{aligned} \tag{C 3}$$

When $\boldsymbol{T}^i$ are defined by (C 2), all the scalar product in brackets in (C 3) are zero, and therefore $\min \widehat{Q} = 0$.

Example 2. Next, consider the network of three vertices in figure 13(*b*). For this network, $\min \widehat{Q} > 0$. To show this, consider the system corresponding to the general system (3.34).

$$(\boldsymbol{T}^1 + \boldsymbol{e}_2)\cdot\boldsymbol{e}_2 = 0, \quad (\boldsymbol{T}^1 - \boldsymbol{T}^2)\cdot\boldsymbol{q}^{12} = 0, \quad (\boldsymbol{T}^1 - \boldsymbol{T}^3)\cdot\boldsymbol{q}^{13} = 0, \tag{C 4a–c}$$

$$(\boldsymbol{T}^2 - \boldsymbol{T}^3)\cdot\boldsymbol{q}^{23} = 0, \quad (\boldsymbol{T}^2 - \boldsymbol{e}_2)\cdot\boldsymbol{e}_2 = 0, \quad (\boldsymbol{T}^3 - \boldsymbol{e}_2)\cdot\boldsymbol{e}_2 = 0. \tag{C 4d–f}$$

We prove that the system (C 4) has no solutions. Indeed, (C 4*e*, *f*) imply $\boldsymbol{T}^2 = t_2\boldsymbol{e}_1 + \boldsymbol{e}_2$, $\boldsymbol{T}^3 = t_3\boldsymbol{e}_1 + \boldsymbol{e}_2$, for some scalars t_2, t_3. Next, (C 4*d*) yields $(t_2 - t_3)\boldsymbol{e}_1\cdot\boldsymbol{q}^{23} = 0$, and thus $t_2 = t_3 = t$. Substituting $\boldsymbol{T}^2 = \boldsymbol{T}^3 = t\boldsymbol{e}_1 + \boldsymbol{e}_2$ into (C 4*b*) and (C 4*c*) we obtain

$$(\boldsymbol{T}^1 - t\boldsymbol{e}_1 - \boldsymbol{e}_2)\cdot\boldsymbol{q}^{12} = 0, \tag{C 5a}$$

$$(\boldsymbol{T}^1 - t\boldsymbol{e}_1 - \boldsymbol{e}_2)\cdot\boldsymbol{q}^{13} = 0. \tag{C 5b}$$

Since $\boldsymbol{q}^{12}, \boldsymbol{q}^{13}$ are non-collinear, (C 5) yields $\boldsymbol{T}^1 = t\boldsymbol{e}_1 + \boldsymbol{e}_2$, which contradicts (C 4*a*).

Example 3. Next, consider a rectangular network of four vertices in figure 13(*c*). The system (3.34) for this example becomes

$$(\boldsymbol{T}^1-\boldsymbol{T}^2)\cdot\boldsymbol{e}_1=0,\quad (\boldsymbol{T}^1-\boldsymbol{T}^4)\cdot\boldsymbol{e}_2=0,\quad (\boldsymbol{T}^2-\boldsymbol{T}^3)\cdot\boldsymbol{e}_2=0,\quad (\boldsymbol{T}^3-\boldsymbol{T}^4)\cdot\boldsymbol{e}_1=0, \tag{C 6a–d}$$

$$(\boldsymbol{T}^1+\boldsymbol{e}_2)\cdot\boldsymbol{e}_2=0,\quad (\boldsymbol{T}^2+\boldsymbol{e}_2)\cdot\boldsymbol{e}_2=0,\quad (\boldsymbol{T}^3-\boldsymbol{e}_2)\cdot\boldsymbol{e}_2=0,\quad (\boldsymbol{T}^4-\boldsymbol{e}_2)\cdot\boldsymbol{e}_2=0. \tag{C 4e–h}$$

Equations (C 6*g*) and (C 6*h*) yield $\boldsymbol{T}^3=t_3\boldsymbol{e}_1+\boldsymbol{e}_2$, $\boldsymbol{T}^4=t_4\boldsymbol{e}_1+\boldsymbol{e}_2$, with some scalars t_3, t_4. Next, (C 6*b*) and (C 6*c*) produce $\boldsymbol{T}^1=t_1\boldsymbol{e}_1+\boldsymbol{e}_2$, $\boldsymbol{T}^2=t_2\boldsymbol{e}_1+\boldsymbol{e}_2$, which contradict, respectively, (C 6*e*) and (C 6*f*).

The three examples above seem to indicate that two basic building blocks for networks with $\widehat{E}>0$ (strong blow-up) are triangles and rectangles aligned with the edges of Ω. Misaligned rectangular structures such as shown in figure 13(*a*), would produce $\widehat{E}=0$ (weak blow-up).

Appendix D. Properties of quasi-triangulated subgraphs

Given an arbitrary network graph Γ, we define its maximal quasi-triangulated subgraph Γ_M by the following iterative procedure.

Step 1. Consider interior vertices which are connected to $\partial\Omega^-$ and call these vertices *generation one* vertices. All interior edges connecting these vertices are *generation one* edges. Add all generation one edges and vertices to the subgraph.

Step 2. Consider all remaining vertices which are connected to the vertices of the subgraph by at least two non-collinear edges. These vertices and edges belong to generation two. Add them to the subgraph. Note that the non-collinearity condition leads to the formation of 'supportive triangles'.

Step 3. Repeat step 2 until no more vertices can be added.

If the maximal quasi-triangulated subgraph Γ_M contains all interior vertices of Γ, we call the graph Γ *quasi-triangulated.* These graphs have the following properties.

PROPOSITION D.1. *Suppose that the network graph Γ is quasi-triangulated. Then there is a unique solution of the system* (3.8)*, up to a horizontal translation.*

PROPOSITION D.2. *Suppose that the boundary conditions are given by* (3.30) *and the network graph Γ contains a backbone. Then Γ is a percolating rigidity graph. Consequently, the extensional effective viscosity $\lambda^\star$ of suspensions corresponding to such networks is $O(\delta^{-3/2})$.*

Proposition D.1 will be proved if we prove the following.

PROPOSITION D.3. *Suppose the network graph Γ is quasi-triangulated. Then every solution of the homogeneous system* (3.12) *is of the form $t\boldsymbol{w}_0$ where t is arbitrary real and $\boldsymbol{w}_0$ is the vector components of which are given by* (3.11).

Proof. First note that (3.12) is the Euler–Lagrange system for the functional

$$Q_{hom}=\tfrac{1}{2}A\boldsymbol{z}\cdot\boldsymbol{z}=\tfrac{1}{2}\sum_{i=1}^{N}\sum_{j\in\mathcal{N}_i}C_{sp}^{ij}((\boldsymbol{T}^i-\boldsymbol{T}^j)\cdot\boldsymbol{q}^{ij})^2+\sum_{i\in I}C_{sp}^{i}(\boldsymbol{T}^i\cdot\boldsymbol{q}^i)^2. \tag{D 1}$$

Clearly the minimum of Q_{hom} is zero. Thus every solution of (3.12) is a minimizer of Q_{hom}. On the other hand, $Q_{hom}(\boldsymbol{T}^1, \ldots, \boldsymbol{T}^N) = 0$ if and only if the vectors $\boldsymbol{T}^i$ satisfy the system of equations

$$(\boldsymbol{T}^i - \boldsymbol{T}^j)\cdot \boldsymbol{q}^{ij} = 0 \quad (i = 1, 2\ldots, N, \quad j \in \mathcal{N}_i) \tag{D 2a}$$

$$\boldsymbol{T}^i \cdot \boldsymbol{q}^i = 0 \quad (i \in I). \tag{D 2b}$$

Therefore, a vector $z = (\boldsymbol{T}^1, \ldots, \boldsymbol{T}^N)^T$ solves (3.12) if and only if $\boldsymbol{T}^i, i = 1, \ldots, N$ solve (D 2). The solvability of (D 2) will be directly linked to the geometric structure of the graph Γ. We begin by observing that $\boldsymbol{q}^i = \pm \boldsymbol{e}_2$. Thus, (D 2*b*) yields

$$\boldsymbol{T}^i = t^i \boldsymbol{e}_1 (i \in I), \tag{D 3}$$

that is, $\boldsymbol{T}^i$ are horizontal for all boundary vertices. Next, consider boundary vertices $\boldsymbol{x}^i, i \in I^-$ (these are vertices connected to $\partial\Omega^-$), and recall that they belong to a path Γ^-, edges of which are interior edges of Γ. Hence, if $i_1 \in I^-$, then there is at least one $i_2 \in I^-, i_2 \neq i_1$ such that $\boldsymbol{x}^{i_1}$ and $\boldsymbol{x}^{i_2}$ are connected by an *interior* edge $b^{i_1 i_2}$. Using (D 2*a*) and (D 3), we obtain

$$(\boldsymbol{T}^{i_1} - \boldsymbol{T}^{i_2})\cdot \boldsymbol{q}^{i_1 i_2} = (t^{i_1} - t^{i_2})\boldsymbol{e}_1 \cdot \boldsymbol{q}^{i_1 i_2} = 0. \tag{D 4}$$

Furthermore, $\boldsymbol{q}^{i_1 i_2}$ is non-vertical, that is, $\boldsymbol{q}^{i_1 i_2}\cdot \boldsymbol{e}_1 \neq 0$, which yields $t^{i_1} = t^{i_2}$. Since each $\boldsymbol{x}^i, i \in I^-$ is connected to at least one other, we obtain

$$\boldsymbol{T}^i = t\boldsymbol{e}_1 \quad (i \in I^-), \tag{D 5}$$

with the same scalar t.

Since the graph is quasi-triangulated, there exists an *interior* vertex $\boldsymbol{x}^{l_1} \in \Gamma$, $\boldsymbol{x}^{l_1} \notin \Gamma^-$, connected to at least two vertices $\boldsymbol{x}^{i_1}, \boldsymbol{x}^{i_2}, i_1, i_2 \in I^-$ by non-collinear edges. Then, using (D 2) we obtain

$$(\boldsymbol{T}^{l_1} - t\boldsymbol{e}_1)\cdot \boldsymbol{q}^{l_1, i_1} = 0, \tag{D 6a}$$

$$(\boldsymbol{T}^{l_1} - t\boldsymbol{e}_1)\cdot \boldsymbol{q}^{l_1, i_2} = 0. \tag{D 6b}$$

Since $\boldsymbol{q}^{l_1, i_1}$ and $\boldsymbol{q}^{l_1, i_2}$ are linearly independent, (D 6) yields $\boldsymbol{T}^{l_1} = t\boldsymbol{e}_1$. Next, let G_1 be the union of Γ^-, $\boldsymbol{x}^{l_1}$ and all the edges which connect $\boldsymbol{x}^{l_1}$ to Γ^-. Using the definition of the quasi-triangulated graph again, we find a vertex $\boldsymbol{x}^{l_2}$, not contained in G_1, and connected to G_1 by two non-collinear edges. Repeating the argument following (D 6), we see that $\boldsymbol{T}^{l_2} = t\boldsymbol{e}_1$. Then we choose G_2 to be the union of G_1, $\boldsymbol{x}^{l_2}$ and all edges of Γ which connect them. Repeating the process we find the vertex $\boldsymbol{x}_{l_3}$ and continue until we obtain

$$\boldsymbol{T}^i = t\boldsymbol{e}_1, \qquad i = 1, \ldots, N \tag{D 7}$$

with the same scalar t. This means that every solution of (D 2) is of the form $t\boldsymbol{w}_0$. Since solution spaces of (D 2) and (3.12) are the same, the proposition is proved. □

The following discrete Korn inequality follows immediately from the Proposition D.3.

COROLLARY D.1. *Suppose that Γ is quasi-triangulated. Let $W \subset \boldsymbol{R}^{2N}$ be the one-dimensional subspace spanned by $\boldsymbol{w}_0$, and let $W^\perp$ denote the orthogonal complement of W in $\boldsymbol{R}^{2N}$. Also, let Q_{hom} and A be, respectively the quadratic form defined in* (D 1) *and its matrix. Then there is a constant $C > 0$ such that the Korn-type inequality*

$$\tfrac{1}{2} Az\cdot z = Q_{hom}(z) \geqslant Cz\cdot z \tag{D 8}$$

holds for all $z \in W^\perp$.

Another straightforward corollary is as follows.

COROLLARY D.2. *Suppose that Γ is quasi-triangulated. Then the system*

$$Az = \boldsymbol{f}$$

has a unique solution $z \in W^{\perp}$ provided $\boldsymbol{f} \perp W$.

Remark. The projection P_W onto the subspace W is defined by

$$P_W \boldsymbol{z} = \frac{\boldsymbol{z} \cdot \boldsymbol{w}_0}{N} \boldsymbol{w}_0.$$

In terms of vectors $\boldsymbol{T}^i$,

$$P_W(\boldsymbol{T}^1, \boldsymbol{T}^2, \ldots, \boldsymbol{T}^N) = \frac{\sum_{i=1}^{n} T_1^i}{N} \boldsymbol{w}_0.$$

Therefore, using the definition of $\boldsymbol{f}$ in terms of $\boldsymbol{R}^i$, we can write the condition $\boldsymbol{f} \perp W$ as

$$\sum_{i=1}^{n} R_1^i = \sum_{i=1}^{N} \boldsymbol{R}^i \cdot \boldsymbol{e}_1 = 0. \tag{D 9}$$

The vectors $\boldsymbol{R}^i$ in (3.10) satisfy (D 9), so that $\boldsymbol{f}$ with R^i defined by (3.10) is orthogonal to W. This gives the unique solvability of the network equations (3.8).

COROLLARY D.3. *Suppose that Γ is quasi-triangulated. Then there is a unique $\boldsymbol{z}^* \in W^{\perp}$ such that every solution of* (3.8) *is of the form $\boldsymbol{z}^* + t\boldsymbol{w}_0$, where $t\boldsymbol{w}_0 \in W$.*

This means that solution of the network equations (3.8) is unique up to a horizontal translation.

Proof of Proposition D.2.

Proof. First we observe that the form $\widehat{Q}$ is a sum of non-negative terms, each of which corresponds to an edge of the network graph Γ. Removal of an edge from Γ corresponds to deletion of one non-negative term in $\widehat{Q}$. This means that for each subgraph Γ' of Γ, $\widehat{Q}(\Gamma) \geqslant \widehat{Q}(\Gamma')$. Next we choose Γ' to be the maximal quasi-triangulated subgraph of Γ. We show that $\min \widehat{Q}(\Gamma') > 0$. Indeed, $\min \widehat{Q}(\Gamma') = 0$ if and only if the corresponding system (3.34) has a solution. To show that this system has no solutions, introduce new unknowns $\hat{\boldsymbol{T}}^i = \boldsymbol{T}^i - \boldsymbol{e}_2$. Then from (3.34), we obtain

$$(\hat{\boldsymbol{T}}^i - \hat{\boldsymbol{T}}^j) \cdot \boldsymbol{q}^{ij} = 0, \tag{D 10}$$

$$\hat{\boldsymbol{T}}^i \cdot \boldsymbol{q}^i = \begin{cases} -2 & \text{when } i \in I^+, \\ 0 & \text{when } i \in I^-. \end{cases} \tag{D 11}$$

Since the vectors $\boldsymbol{q}^i$, are vertical, (D 11) yields

$$\hat{\boldsymbol{T}}^i = t^i \boldsymbol{e}_1 \quad (i \in I^-), \tag{D 12}$$

where t^i is a constant. Recall that Γ contains a path Γ^- which consists of all boundary vertices connected to $\partial\Omega^-$ and all interior edges connecting these vertices. Hence, each $\boldsymbol{x}^{i_1}, i_1 \in I^-$ has a neighbour $\boldsymbol{x}^{i_2}, i_2 \in I^-$ and thus $(t^{i_1} - t^{i_2})\boldsymbol{e}_1 \cdot \boldsymbol{q}^{i_1 i_2} = 0$ from (D 10). Since two boundary vertices cannot be joined by a vertical edge, $\boldsymbol{e}_1 \cdot \boldsymbol{q}^{i_1 i_2} \neq 0$.

This implies that all $t^i, i \in I^-$ are equal, that is

$$\hat{\boldsymbol{T}}^i = t\boldsymbol{e}_1 \quad (i \in I^-), \tag{D 13}$$

where t is a constant. Next, consider the boundary path Γ^-. By definition of Γ' there is a vertex $\boldsymbol{x}^{j_1}$, $j_1 \notin I^-$ connected to the boundary vertices $\boldsymbol{x}^{i_1}$, $\boldsymbol{x}^{i_2}$, $i_1, i_2 \in I^-$ by non-collinear edges of Γ. Then from (D 10) and (D 13) we have

$$(\hat{\boldsymbol{T}}^{j_1} - t\boldsymbol{e}_1)\cdot \boldsymbol{q}^{j_1,i_1} = 0,$$
$$(\hat{\boldsymbol{T}}^{j_1} - t\boldsymbol{e}_1)\cdot \boldsymbol{q}^{j_1,i_2} = 0.$$

Since $\boldsymbol{q}^{j_1,i_1}$ and $\boldsymbol{q}^{j_1,i_2}$ are linearly independent, we obtain $\hat{\boldsymbol{T}}^{j_1} = t\boldsymbol{e}_1$. Now this argument can be used recursively. Next we choose G_1 to be the union of vertices $\boldsymbol{x}^i, i \in I^-$, $\boldsymbol{x}^{j_1}$ and the edges of Γ' which connect these vertices. Repeating the argument, we find a vertex $\boldsymbol{x}^{j_2} \notin G_1$, connected to at least two vertices of G_1 by non-collinear edges, which yields $\hat{\boldsymbol{T}}^{j_2} = t\boldsymbol{e}_1$, and so on, until we obtain $\hat{\boldsymbol{T}}^i = t\boldsymbol{e}_1$ for all vertices $\boldsymbol{x}^i$ which belong to Γ'. By assumption, Γ' contains at least one vertex $\boldsymbol{x}^+ \in I^+$; but then $\hat{\boldsymbol{T}}^+ \cdot \boldsymbol{q}^+ = -t\boldsymbol{e}_1 \cdot \boldsymbol{e}_2 = 0$ which contradicts (D 11). This contradiction shows that the system (D 10), (D 11) has no solutions. □

Appendix E. Strong and weak blow-up for rectangular networks

PROPOSITION E.1. *Suppose that a network graph Γ contains a path $P^{\pm}$ such that*
(i) it connects $\partial\Omega^+$ and $\partial\Omega^-$,
(ii) all edges of $P^{\pm}$ are vertical.
Then Γ is a percolating rigidity graph.

Proof. First, we note that if a path $P^{\pm}$ has percolating rigidity, then the 'larger' graph Γ is also a percolating rigidity graph. Therefore, we need only show that a path of vertical edges has percolating rigidity, that is, the quadratic form $\widehat{Q}$ corresponding to such a path is positive-definite.

For simplicity, consider a path containing three vertices. The argument can be directly generalized to an arbitrary number of vertices. The general strategy in suggested in § 3.3.2 is to study the system (3.34). If this system has no solutions, then (3.5) must hold. In the present case, (3.34) has the form

$$(\boldsymbol{T}^1 - \boldsymbol{e}_2)\cdot \boldsymbol{e}_2 = 0, \tag{E 1a}$$
$$(\boldsymbol{T}^1 - \boldsymbol{T}^2)\cdot \boldsymbol{e}_2 = 0, \tag{E 1b}$$
$$(\boldsymbol{T}^2 - \boldsymbol{T}^3)\cdot \boldsymbol{e}_2 = 0, \tag{E 1c}$$
$$(\boldsymbol{T}^3 + \boldsymbol{e}_2)\cdot \boldsymbol{e}_2 = 0. \tag{E 1d}$$

Introduce new unknown vectors $\widehat{\boldsymbol{T}}^i = \boldsymbol{T}^i + \boldsymbol{e}_2$ $(i = 1, 2, 3)$. Equation (E 1*d*) yields $\widehat{\boldsymbol{T}}^3 = t_3\boldsymbol{e}_1$, where t_3 is a scalar. Then from (E1 *c*) we obtain $\widehat{\boldsymbol{T}}^2 = t_2\boldsymbol{e}_1$, and then yields $\widehat{\boldsymbol{T}}^1 = t_1\boldsymbol{e}_1$, which contradicts (E 1*a*). The contradiction shows that the system (E 1*b*) has no solutions. The argument can easily be modified to show that if at least one of the edges of a path is non-vertical, then this path does not have percolating rigidity. □

Next, we present a proof that the network in figure 12 produces weak blow-up. The argument admits a straightforward generalization to a network with an arbitrary

number of vertices. We begin by considering a single path connecting $\partial\Omega^+$ and $\partial\Omega^-$. This path may be any of the three such paths in figure 12.

The system (3.34) written for the path has the form

$$(\boldsymbol{T}^1 - \boldsymbol{e}_2)\cdot\boldsymbol{e}_2 = 0, \tag{E 2a}$$
$$(\boldsymbol{T}^1 - \boldsymbol{T}^2)\cdot\boldsymbol{k} = 0, \tag{E 2b}$$
$$(\boldsymbol{T}^2 - \boldsymbol{T}^3)\cdot\boldsymbol{k} = 0, \tag{E 2c}$$
$$(\boldsymbol{T}^3 - \boldsymbol{T}^4)\cdot\boldsymbol{k} = 0, \tag{E 2d}$$
$$(\boldsymbol{T}^4 + \boldsymbol{e}_2)\cdot\boldsymbol{e}_2 = 0. \tag{E 2e}$$

For technical reasons it is convenient to introduce new unknowns $\boldsymbol{u}_1 = \boldsymbol{T}^1 - \boldsymbol{e}_2$, $\boldsymbol{u}_{12} = \boldsymbol{T}^1 - \boldsymbol{T}^2$, $\boldsymbol{u}_{23} = \boldsymbol{T}^2 - \boldsymbol{T}^3$, $\boldsymbol{u}_{34} = \boldsymbol{T}^3 - \boldsymbol{T}^4$. The relations between $\boldsymbol{u}_{ij}$ and $\boldsymbol{T}^i$ are

$$\boldsymbol{T}^1 = \boldsymbol{u}_1 + 2\boldsymbol{e}_2, \tag{E 3a}$$
$$\boldsymbol{T}^2 = \boldsymbol{u}_1 + 2\boldsymbol{e}_2 - \boldsymbol{u}_{12}, \tag{E 3b}$$
$$\boldsymbol{T}^3 = \boldsymbol{u}_1 + 2\boldsymbol{e}_2 - \boldsymbol{u}_{12} - \boldsymbol{u}_{23}, \tag{E 3c}$$
$$\boldsymbol{T}^4 = \boldsymbol{u}_1 + 2\boldsymbol{e}_2 - \boldsymbol{u}_{12} - \boldsymbol{u}_{23} - \boldsymbol{u}_{34}. \tag{E 3d}$$

From (E 2*a–d*) we see that $\boldsymbol{u}_1 = t_1\boldsymbol{e}_1$, and $\boldsymbol{u}_{i,i+1} = t_{i,i+1}\boldsymbol{k}^\perp$, $i = 1, 2, 3$, where $\boldsymbol{k}^\perp$ denotes a unit vector orthogonal to $\boldsymbol{k}$, and $t_1, t_{i,i+1}$ are scalars. The problems of solving (E 2) is now reduced to finding $t_1, t_{i,i+1}$ such that (E 2*e*) is satisfied. Equation (E 2*e*) shows that

$$\boldsymbol{T}^4 = t_4\boldsymbol{e}_1 - \boldsymbol{e}_2, \tag{E 4}$$

where t_4 is a scalar. Equating (E 4) and (E 3), we obtain the equation for $t_1, t_{12}, t_{23}, t_{34}$ and t_4:

$$t_4\boldsymbol{e}_1 = t_1\boldsymbol{e}_1 + \boldsymbol{e}_2 - (t_{12} + t_{23} + t_{34})\boldsymbol{k}^\perp. \tag{E 5}$$

This yields two scalar equations

$$0 = 1 - (t_{12} + t_{23} + t_{34})\boldsymbol{k}^\perp\cdot\boldsymbol{e}_2, \tag{E 6}$$

and

$$t_1 - t_4 = (t_{12} + t_{23} + t_{34})\boldsymbol{k}^\perp\cdot\boldsymbol{e}_1. \tag{E 7}$$

The system of two equations (E 6), (E 7) for five unknowns has infinitely many non-trivial solutions as long as $\boldsymbol{k}^\perp\cdot\boldsymbol{e}_2 \neq 0$, that is, the interior edges of the path are non-vertical.

At the next step of construction, we consider the full lattice in figure 12 containing 12 vertices. The interior edges of the graph are oriented either by the unit vector $\boldsymbol{k}$ as above (longitudinal edges), or by $\boldsymbol{k}^\perp$ (latitudinal edges). We view the graph as the union of three paths of longitudinal edges extending from $\partial\Omega^-$ to $\partial\Omega^+$, with latitudinal edges connecting these paths. To obtain the desired example, we choose the velocities $\boldsymbol{T}^i$ for one of the paths, as explained above. Then we prescribe the same velocities to the corresponding vertices of two remaining paths. Now, if two neighbours $\boldsymbol{x}^i$, $\boldsymbol{x}^j$ belong to different paths, then $\boldsymbol{T}^i = \boldsymbol{T}^j$, so the corresponding equation $(\boldsymbol{T}^i - \boldsymbol{T}^j)\cdot\boldsymbol{k}^\perp = 0$ of the system (3.34) is satisfied. When the neighbours $\boldsymbol{x}^i$, $\boldsymbol{x}^j$ belong to the same path, the corresponding equation $(\boldsymbol{T}^i - \boldsymbol{T}^j)\cdot\boldsymbol{k} = 0$ is satisfied by the choice of $\boldsymbol{T}^i$, $\boldsymbol{T}^j$. Therefore, the whole system (3.34) in this case has infinitely many non-trivial solutions. Each of these solutions makes $\widehat{Q}$, and thus the leading term in the asymptotics of $\lambda^\star$, zero.

REFERENCES

Bakhvalov, N. & Panasenko, G. 1989 *Homogenization: Averaging Processes in Periodic Media.* Kluwer.

Ball, R. C. & Melrose, J. R. 1997*a* A simulation technique for many spheres in quasi-static motion under frame-invariant pair drag and Brownian forces. *Physica* A **247**, 444–472.

Ball, R. C. & Melrose, J. R. 1997*b* Colloidal microdynamics: pair-drag simulations of model-concentrated aggregated systems. *Phys. Rev.* E **56**, 7067–7077.

Batchelor, G. K. & Green, J. T. 1972 The determination of the bulk stress in a suspension of spherical particles to order c^2. *J. Fluid Mech.* **56**, 401–427.

Bensoussan, A., Lions, J. L., & Papanicolaou, G. 1978 *Asymptotic Analysis in Periodic structures.* North-Holland.

Berlyand, L. & Kolpakov, A. 2001 Network approximation in the limit of small inter-particle distance of the effective properties of a high-contrast random dispersed composite. *Arch. Rat. Mech. Anal.* **159**, 179–227.

Berlyand, L., Borcea, L. & Panchenko, A. 2005*a* Network approximation for effective viscosity of concentrated suspensions with complex geometries. *SIAM J. Math. Anal.* **36**, 1580–1628.

Berlyand, L., Gorb, Y. & Novikov, A. 2005*b* Fictitious fluid approach and anomalous blow-up of the dissipation rate in 2D model of concentrated suspensions (submitted).

Brady, J. F. & Morris, J. F. 1997 Microstructure of strongly sheared suspensions and its impact on rheology and diffusion. *J. Fluid Mech.* **348**, 103–139.

Carreau, P. J. & Cotton, F. 2002 Rheological properties of concentrated suspensions. In *Transport Processes in Bubbles, Drops and Particles* (ed. D. De Kee & R. P. Chhabra). Taylor & Francis.

Coussot, P. 2002 Flows of concentrated granular mixtures. In *Transport processes in Bubbles, Drops and Particles* (ed. D. De Kee & R. P. Chhabra). Taylor & Francis.

Edelsbrunner, H. 2000 Triangulations and meshes in computational geometry. *Acta Numerica*, 1–81.

Einstein, A. 1906*a* Eine neue Bestimmung der Moleküldimensionen. *Annln. Phys.* **19**, 289.

Einstein, A. 1906*b* Eine neue Bestimmung der Moleküldimensionen. *Annln. Phys.* **34**, 591.

Frankel, N. A. & Acrivos, A. 1967 On the viscosity of a concentrated suspension of solid spheres. *Chem. Engng Sci.* **22**, 847–853.

Jikov, V., Kozlov, S. & Oleinik, O. 1994 *Homogenization of Differential Operators and Integral Functionals.* Springer.

Kim, S. & Karilla, S. J. 1991 *Microhydrodynamics: Principles and Selected Applications.* Butterworth–Heinemann.

Nunan. K. C. & Keller, J. B. 1984 Effective viscosity of periodic suspensions *J. Fluid Mech.* **142**, 269–287.

Sanchez-Palencia, E. 1980 *Non-homogeneous Media and Vibration Theory*. Springer.

Schowalter, W. R. 1978 *Mechanics of Non-Newtonian Fluids.* Pergamon.

Shikata, T. & Pearson, D. S. 1994 Viscoelastic behavior of concentrated spherical suspensions. *J. Rheol.* **38**, 601–616.

Shook, C. A. & Roco, M. C. 1991 *Slurry Flow. Principles and Practice* Butterworth-Heinemann.

Sierou, A. & Brady, J. F. 2001 Accelerated Stokesian dynamic simulations. *J. Fluid Mech.* **448**, 115–146.

Sierou, A. & Brady, J. F. 2002 Rheology and microstructure in concentrated noncolloidal suspensions. *J. Rheol.* **46**, 1031–1056.

Stickel, J. J. & Powell, R. L. 2005 Fluid mechanics and rheology of dense suspensions. *Annu. Rev. Fluid Mech.* **37**, 129–149.

Van der Werff, J. C., de Kruif, C. G., Blom, C. & Mellema, J. 1989 Linear viscoelastic behavior of dense hard-sphere dispersions. *Phys. Rev.* A **39**, 795–807.